

## Comparisons between shell-model calculations, seniority truncation, and quasiparticle approximations: Application to the odd Ni isotopes and odd $N = 82$ isotones

L. Losano

*Departamento de Física, Universidade Federal da Paraíba, João Pessoa, Brazil*

H. Dias

*Instituto de Física, Universidade de São Paulo, São Paulo, Brazil*

F. Krmpotić

*Departamento de Física, Universidad Nacional de La Plata, La Plata, Argentina*

B. H. Wildenthal

*Department of Physics and Astronomy, University of New Mexico, Albuquerque, New Mexico 87131*

(Received 6 June 1988)

A detailed study of the results of correcting BCS approximation for the effects of particle-number projection and blocking has been carried out. A low-seniority shell-model approximation was used as the frame of reference for investigating the mixing of one- and three-quasiparticle states in odd-mass Ni isotopes and in odd-mass  $N = 82$  isotones. We discuss the results obtained for the energy spectra and electromagnetic decay properties. Effects of seniority-five configurations on the low-lying states have also been studied through the comparison of the low-seniority shell-model results with those which arose from the corresponding full shell-model calculations.

### I. INTRODUCTION

Because of the large dimensionalities inherent in the shell model, the only practical approaches within this framework to treating the structure of medium and heavy nuclei with open shells are based on the quasiparticle BCS approximation. The effects of spurious states due to the nonconservation of the number of particles in the quasiparticle method can be removed, although only partially, by following the procedure of Kuo *et al.*<sup>1</sup> The complete elimination of such spurious states can be achieved through carrying out the projection of particle number,<sup>2-6</sup> in the formalism referred to as the projected BCS approximation (PBCS). However, with the PBCS technique much of the physical transparency which is a prominent advantage of the simple BCS method is lost.

Furthermore, the PBCS approach does not take into account the fact that pairing correlations may be different for different nuclear states. In the PBCS formalism the diffuseness of the Fermi-energy surface for all states in a spectrum is identical to that determined for the BCS ground state. However, we know that the Fermi surface should become sharper as the number of quasiparticles increases, and that pairing correlations vanish completely in highly excited states. Thus, the BCS and PBCS methods should be corrected by carrying out a new energy minimization for each state. The importance of this correction, usually called the blocking effect, in treating odd-mass nuclei, was first pointed out and discussed qualitatively by Nilsson.<sup>7</sup> The BCS formalism as corrected for blocking effects (BBCS) retains most of the simplicity of the BCS method, but it still contains the effects of

spuriousity related to the nonconservation of particle number.

Several studies which compare the BCS and PBCS methods as applied to the properties of odd-mass nuclei have been done.<sup>3-6</sup> However, no similar study has been performed of the effects of blocking within the BCS formalism, even though the BCS method is much more transparent than the PBCS formalism. The relative importance of the effects of blocking and number projection, i.e., a comparison between the BBCS and PBCS method, is also an open question. An initial study<sup>8</sup> for the three-valence-particle nucleus  $^{135}_{53}\text{I}_{82}$  has compared different BCS approximations within the model space of one and three quasiparticles (1qp + 3qp) with exact calculations. The results suggest that the effects of blocking and number projection may play an important role in the description of low-lying states in odd-mass nuclei. Studies in a similar view of nuclei with more than three valence particles have not been done.

The principal aim of the present work is to study the results of correcting the BCS approximation the effects of particle-number projection and blocking. We study the low-lying states of odd-mass nuclei as described within the 1qp + 3qp subspace. In order to establish the frame of reference for these studies we also describe the same nuclei with exact shell-model calculations which use the same set of Hamiltonian parameters. The results for two different shell-model calculations will be presented. In the first set of results, only configurations states with seniority ( $\nu$ ) equal to or smaller than three were included in the space. This approach, which will be called the low-seniority shell model (LSSM), is the exact limit for all

BCS approximations within the subspace of  $1q_p + 3q_p$ . In the second set of results, the model space consisted of the complete set of configuration states for the active single-particle orbits. From the comparison of these complete shell-model (CSM) results with the LSSM results we are able to infer the extent to which the configurations with  $\nu=5$  participate in the structure of low-lying states. A comparison with experimental data is not our aim here, but this will be the subject of a forthcoming paper in which the method explained here will be used.<sup>9</sup>

In Sec. II we describe the different BCS formalisms. The shell-model formalism is fully discussed in the literature<sup>10,11</sup> and will not be described here. In Sec. III, we give details of the numerical calculations. In Sec. IV A we compare the CSM and LSSM calculations to study the effects of configurations with  $\nu=5$  on the structure of the low-lying states. In Sec. IV B the influence of configurations with  $\nu=3$  and 1 and with a number of quasiparticles  $N_{qp}$  higher than five is studied by comparison of the LSSM with the PBCS calculations. In Sec. IV C we discuss the effects induced by the BBCS and PBCS corrections. General conclusions are drawn in Sec. V.

## II. FORMALISM

### A. Evaluation of the matrix elements

In order to calculate the matrix elements of the shell-model Hamiltonian,

$$\mathcal{H} = \sum_{\alpha} \epsilon_{\alpha} a_{\alpha}^{\dagger} a_{\alpha} + \frac{1}{4} \sum_{\alpha\beta\gamma\delta} \langle \alpha\beta | v | \gamma\delta \rangle a_{\alpha}^{\dagger} a_{\beta}^{\dagger} a_{\delta} a_{\gamma}, \quad (2.1)$$

and of the one-body operators,

$$T_{\lambda\mu} = \sum_{\alpha\beta} \langle \alpha | T_{\lambda\mu} | \beta \rangle a_{\alpha}^{\dagger} a_{\beta}, \quad (2.2)$$

where  $a_{\alpha}^{\dagger} (a_{\alpha})$  are particle creation (destruction) operators and  $\alpha \equiv (j_a, m_a)$  and  $\bar{\alpha} = (-)^{j_a - m_a} (j_a, -m_a)$ , we introduce a  $z$ -dependent canonical transformation<sup>8</sup>

$$\begin{aligned} d_{\alpha} &= \sqrt{\sigma_{\alpha}} (u_{\alpha} a_{\alpha} - z v_{\alpha} a_{\bar{\alpha}}^{\dagger}), \\ d_{\bar{\alpha}}^* &= \sqrt{\sigma_{\alpha}} (u_{\alpha}^* a_{\alpha}^{\dagger} - z v_{\alpha}^* a_{\bar{\alpha}}), \end{aligned} \quad (2.3)$$

with

$$\sigma_{\alpha} = (u_{\alpha} u_{\alpha}^* + z^2 v_{\alpha} v_{\alpha}^*)^{-1}. \quad (2.4)$$

Here,  $(u_{\alpha}, v_{\alpha})$  and  $(u_{\alpha}^*, v_{\alpha}^*)$  are the BCS parameters in the ket states and bra states, respectively, and the symbol  $*$  on the creation operator  $d_{\alpha}^*$  stands for the Hermitian conjugation ( $\dagger$ ) plus the transformation  $(u_{\alpha}, v_{\alpha}) \leftrightarrow (u_{\alpha}^*, v_{\alpha}^*)$ . It is easy to see that

$$\{d_{\alpha}^*, d_{\beta}\} = \delta_{\alpha\beta} \quad (2.5)$$

and

$$d_{\alpha} |0; z\rangle = \langle 0; z | d_{\alpha}^* = 0, \quad (2.6)$$

where

$$|0; z\rangle = \prod_{\alpha>0} (u_{\alpha} + z v_{\alpha} a_{\alpha}^{\dagger} a_{\bar{\alpha}}^{\dagger}) |0\rangle, \quad (2.7)$$

and  $|0\rangle$  represents the particle vacua.

By means of the inverse transformation

$$a_{\alpha}^{\dagger} = \sqrt{\sigma_{\alpha}} (u_{\alpha} d_{\alpha}^* + z v_{\alpha} d_{\bar{\alpha}}), \quad (2.8a)$$

$$a_{\alpha} = \sqrt{\sigma_{\alpha}} (u_{\alpha}^* d_{\alpha} + z v_{\alpha} d_{\bar{\alpha}}^*), \quad (2.8b)$$

the Hamiltonian reads

$$\begin{aligned} \mathcal{H} &= \mathcal{H}_{00} + \mathcal{H}_{11} + \mathcal{H}_{20} + \mathcal{H}_{20}^* + \mathcal{H}_{22} \\ &\quad + \mathcal{H}_{31} + \mathcal{H}_{31}^* + \mathcal{H}_{40} + \mathcal{H}_{40}^*, \end{aligned} \quad (2.9)$$

with

$$\mathcal{H}_{00} = \sum_{\alpha} \hat{a}^2 \sigma_{\alpha} z^2 [v_{\alpha} v_{\alpha}^* (\epsilon_{\alpha} - \frac{1}{2} \mu_{\alpha}) - \frac{1}{2} u_{\alpha} v_{\alpha}^* \Delta_{\alpha}], \quad (2.10a)$$

$$\begin{aligned} \mathcal{H}_{11} &= - \sum_{\alpha} \hat{a} \sigma_{\alpha} [(u_{\alpha} u_{\alpha}^* - z^2 v_{\alpha} v_{\alpha}^*) (\epsilon_{\alpha} - \mu_{\alpha}) \\ &\quad + z^2 (u_{\alpha} v_{\alpha}^* \Delta_{\alpha} + u_{\alpha}^* v_{\alpha} \Delta_{\alpha}^*)] \bar{D}_{00}(aa), \end{aligned} \quad (2.10b)$$

$$\begin{aligned} \mathcal{H}_{20} &= \sum_{\alpha} \hat{a} \sigma_{\alpha} [z u_{\alpha} v_{\alpha} (\epsilon_{\alpha} - \mu_{\alpha}) \\ &\quad - \frac{1}{2} (u_{\alpha}^2 \Delta_{\alpha} - z^2 v_{\alpha}^2 \Delta_{\alpha}^*)] D_{00}^*(aa), \end{aligned} \quad (2.10c)$$

$$\begin{aligned} \mathcal{H}_{22} &= \frac{1}{8} \sum_{\substack{abcd \\ JM}} (\sigma_{\alpha} \sigma_b \sigma_c \sigma_d)^{1/2} [(u_{\alpha} u_b u_c^* u_d^* \\ &\quad + z^4 v_{\alpha} v_b v_c^* v_d^*) g_J(abcd) \\ &\quad + 4z^2 u_{\alpha} v_b u_c^* u_d^* f_J(abcd)] \\ &\quad \times D_{JM}^*(ab) D_{JM}(cd), \end{aligned} \quad (2.10d)$$

$$\begin{aligned} \mathcal{H}_{31} &= -\frac{1}{4} \sum_{\substack{abcd \\ JM}} (\sigma_{\alpha} \sigma_b \sigma_c \sigma_d)^{1/2} z g_J(bacd) \\ &\quad \times (u_{\alpha} u_b u_c^* v_d - z^2 v_{\alpha} v_b v_c^* v_d) \\ &\quad \times (-)^{J+M} D_{J-M}^*(ba) \bar{D}_{JM}(cd), \end{aligned} \quad (2.10e)$$

$$\begin{aligned} \mathcal{H}_{40} &= -\frac{1}{8} \sum_{\substack{abcd \\ JM}} (\sigma_{\alpha} \sigma_b \sigma_c \sigma_d)^{1/2} z^2 g_J(bacd) u_{\alpha} u_b v_c v_d \\ &\quad \times (-)^{J+M} D_{J-M}^*(ba) D_{JM}^*(cd), \end{aligned} \quad (2.10f)$$

where the operators  $\bar{D}_{JM}(ab)$  and  $D_{JM}^*(ab)$  are defined as

$$\bar{D}_{JM}(ab) = \sum_{m_a m_b} (j_a m_a j_b m_b | JM) d_{\alpha}^* d_{\bar{\alpha}} \quad (2.11a)$$

and

$$\begin{aligned} D_{JM}^*(ab) &\equiv [D_{JM}(ab)]^* \\ &= \sum_{m_a m_b} (j_a m_a j_b m_b | JM) d_{\beta}^* d_{\alpha}^*. \end{aligned} \quad (2.11b)$$

The gap parameters  $\Delta_{\alpha}$  and the chemical potentials  $\mu_{\alpha}$  are given by

$$\Delta_{\alpha} = -\frac{1}{4} z \hat{a}^{-1} \sum_c \hat{c} g_0(aacc) \sigma_c v_c u_c^*, \quad (2.12)$$

and

$$\mu_a = -\frac{1}{2}z\hat{a}^{-1} \sum_c \hat{c} f_0(aacc) \sigma_c v_c v_c^* . \quad (2.13)$$

The quantities  $f_J(abcd)$  and  $g_J(abcd)$  are antisymmetrized matrix elements of the interaction<sup>3</sup> and  $\hat{a} \equiv (2j_a + 1)^{1/2}$ .

In the same way the transition operator (2.2) takes the form

$$\begin{aligned} T_{\lambda\mu} = & -\hat{\lambda}^{-1} \sum_{ab} (\sigma_a \sigma_b)^{1/2} \langle a || T_{\lambda} || b \rangle \\ & \times \{ [ (-)^x u_a u_b^* - z^2 v_a^* v_b ] \bar{D}_{\lambda\mu}(ab) \\ & + \frac{1}{2} z [ u_a v_b + (-)^x v_a u_b ] D_{\lambda\mu}^*(ab) \\ & + \frac{1}{2} z [ v_a^* v_b^* + (-)^x v_a^* v_b^* ] D_{\lambda\bar{\mu}}(ab) \} \\ & + \delta_{\lambda 0} \delta_{\mu 0} \sum_a \hat{a} v_a v_a^* \sigma_a \langle a || T_{\lambda} || a \rangle , \end{aligned} \quad (2.14)$$

where  $x=0$  and  $1$  for electric and magnetic moments, respectively.

The generating wave functions<sup>3</sup> are rewritten as

$$| \alpha ; z \rangle = \sqrt{\sigma_a} z d_{\alpha}^* | 0, z \rangle , \quad (2.15a)$$

for a one-quasiparticle state (1qp),

$$\begin{aligned} | (ab)JM ; z \rangle = & (\sigma_a \sigma_b)^{1/2} \\ & \times [ z^2 D_{JM}^*(ab) - \delta_{J0} \delta_{ab} \hat{a} z \\ & \times (u_a v_a^* z^2 - v_a u_a^*) ] | 0, z \rangle , \end{aligned} \quad (2.15b)$$

for a two-quasiparticle state (2qp) and

$$\begin{aligned} | [(ab)J,c]IM ; z \rangle = & (\sigma_a \sigma_b \sigma_c)^{1/2} \\ & \times \left[ z^3 \sum_{Mm_{\gamma}} (JMj_c m_{\gamma} | IM) d_{\gamma}^* D_{JM}^*(ab) \right. \\ & \left. - z^2 H(abJc, I) d_{IM}^* \right] | 0 ; z \rangle , \end{aligned} \quad (2.15c)$$

for a three-quasiparticle state (3qp). Here

$$\begin{aligned} H(abJc ; I) = & \delta_{J0} \delta_{ab} \delta_{cI} \hat{a} (u_a v_a^* z^2 - v_a u_a^*) \\ & - \hat{J} \hat{I}^{-1} \delta_J(ab ; cI) (u_c v_c^* z^2 - v_c u_c^*) \end{aligned} \quad (2.16)$$

and

$$\delta_J(ab, cd) = \delta_{ac} \delta_{bd} - (-)^{J+j_a+j_b} \delta_{ab} \delta_{bc} . \quad (2.17)$$

Utilizing the anticommutation relation (2.5), the matrix elements of the operators (2.1) and (2.2) are easily calculated.<sup>12</sup>

It should be noted that our formalism for blocking differs from the one introduced by Allaart and Van Gunsteren<sup>5</sup> in that their quasiparticle transformation is not canonical.

The results for the BCS, BBCS, and PBCS methods are obtained with the above-mentioned formulas under the following conditions:

$$\begin{aligned} u_a^* &= u_a, \quad v_a^* = v_a \text{ (PBCS) ,} \\ z &= 1 \text{ (BBCS) ,} \\ u_a^* &= u_a, \quad v_a^* = v_a, \text{ and } z = 1 \text{ (BCS) .} \end{aligned}$$

## B. Residual interaction

In this work we utilize an interaction for which the gap equations, discussed below, are very similar to those of the pairing force, viz., the surface delta interaction (SDI).<sup>13</sup> Because of this, the calculation of the pairing parameters  $u_a$  and  $v_a$  is greatly simplified in the formalisms which include the effects of blocking.

The SDI has the form

$$V(1,2) = -4\pi G \delta(\Omega_{12}) \delta(r_1 - R) \delta(r_2 - R) , \quad (2.18)$$

where  $G$  is the coupling strength,  $\Omega_{12}$  is the angular coordinate between the interacting particles 1 and 2, and  $R$  is the nuclear radius. The corresponding matrix elements for pair scattering are

$$\begin{aligned} g_J(abcd) = & G \hat{a} \hat{b} \hat{c} \hat{d} (-)^{l_a+l_c+j_b+j_d} i^{l_c+l_d+l_a+l_b} \\ & \times \begin{bmatrix} J_a & J_b & J \\ \frac{1}{2} & -\frac{1}{2} & 0 \end{bmatrix} \begin{bmatrix} J_c & J_d & J \\ \frac{1}{2} & -\frac{1}{2} & 0 \end{bmatrix} \\ & \times [ 1 + (-)^{l_c+l_d+J} ] . \end{aligned} \quad (2.19)$$

In solving the gap equations one needs the matrix elements

$$g_0(aabb) = -2G \hat{a} \hat{b} , \quad (2.20a)$$

and

$$f_0(aabb) = -G \hat{a} \hat{b} . \quad (2.20b)$$

The corresponding matrix elements for the pairing force are

$$g_0(aabb) = -2G \hat{a} \hat{b} \quad (2.21a)$$

and

$$f_0(aabb) = -2G \delta_{ab} . \quad (2.21b)$$

## C. Gap equations

In order to establish the gap equations for the state  $|\eta\rangle$ , which may contain zero, one, . . . , etc., quasiparticles, we always start from the variational statements

$$\delta \langle \eta | \mathcal{H}(\lambda) | \eta \rangle = 0 , \quad (2.22a)$$

$$\langle \eta | N | \eta \rangle = n_0 , \quad (2.22b)$$

where

$$\mathcal{H}(\lambda) = \mathcal{H} - \lambda N , \quad (2.23)$$

$n_0$  is the number of valence particles,  $\lambda$  is the chemical potential, and  $N$  is the particle-number operator.

Within the BCS and PBCS formalism all the pairing properties are defined in the BCS vacuum ( $|\eta\rangle \equiv |0; z=1\rangle$ ). From expressions (2.22) one obtains the standard gap equations for the parameters  $u_s$  and  $v_s$ ,

$$2u_s v_s (\epsilon_s - \mu_s - \lambda) - (u_s^2 - v_s^2) \Delta_s = 0 , \quad (2.24a)$$

$$\sum_r \hat{r}^2 v_r^2 = n_0 . \quad (2.24b)$$

When the effects of blocking are considered, the state  $|\eta\rangle$  is no longer the BCS vacuum but instead, the

blocked state, and the gap equations change correspondingly. In the case of 1qp, the gap equations for the quasiparticle in the state  $(|\eta\rangle = |\alpha; z=1\rangle)|\alpha\rangle$  become

$$[2u_s v_s (\epsilon_s - \mu_s - \lambda) - \Delta_s (u_s^2 - v_s^2)] (1 - 2\hat{s}^{-2} \delta_{sa}) - \frac{(u_s^2 - v_s^2) u_a v_a}{2\hat{a}\hat{s}} g_0(aass) + \frac{2u_s v_s u_a^2 v_a^2}{\hat{a}\hat{s}} f_0(aass) = 0, \quad (2.25a)$$

$$\sum_r (\hat{r}^2 - 2\delta_{ar}) v_r^2 = n_0 - 1. \quad (2.25b)$$

Note that for  $j_s = j_a = \frac{1}{2}$  these equations do not allow us to determine the values of the parameters  $u_{1/2}$  and  $v_{1/2}$ .

This fact, however, is irrelevant because when the blocked particle is in the state  $j_a = \frac{1}{2}$  the quantities  $u_{1/2}$  and  $v_{1/2}$  do not appear explicitly in the calculation. This can be seen from (2.15a) which, for  $j_a = \frac{1}{2}$ , reads

$$|\frac{1}{2}m; z\rangle = z a_{(1/2)m}^\dagger \prod_{\substack{\alpha > 0 \\ j_a \neq \frac{1}{2}, m_a \neq \frac{1}{2}}} (u_a + z_a v_a a_{\alpha}^\dagger a_{\bar{\alpha}}^\dagger) |0\rangle. \quad (2.26)$$

Before going to the 3qp case it is convenient to discuss the gap equations for two quasiparticles. If the blocked states are  $|\alpha\rangle$  and  $|\beta\rangle$ ,  $(|\eta\rangle = |(ab)JM; z=1\rangle)$ , then Eqs. (2.22) lead to

$$[2u_s v_s (\epsilon_s - \mu_s - \lambda) - \Delta_s (u_s^2 - v_s^2)] \left[ 1 - \frac{2}{\hat{s}^2} (\delta_{sa} + \delta_{sb}) \right] - \frac{(u_s^2 - v_s^2)}{2} \left[ \frac{u_a v_a}{\hat{a}\hat{s}} g_0(aass) + \frac{u_b v_b}{\hat{b}\hat{s}} g_0(bbss) \right] + u_s v_s \left[ \frac{(u_a^2 - v_a^2)}{\hat{a}\hat{s}} f_0(aass) + \frac{(u_b^2 - v_b^2)}{\hat{b}\hat{s}} f_0(bbss) \right] + \frac{u_s v_s}{(1 + \delta_{ab}) \hat{s}^2} [(u_b^2 - v_b^2) \delta_{sa} + (u_a^2 - v_a^2) \delta_{sb}] [g_J(abab) + f_J(abab)] - \frac{(u_s^2 - v_s^2)}{(1 + \delta_{ab}) \hat{s}^2} f_J(abba) (-)^{j_a + j_b + J} (u_b v_b \delta_{sa} + u_a v_a \delta_{sb}) = 0, \quad (2.27a)$$

$$\sum_r [\hat{r}^2 - 2(\delta_{ra} + \delta_{rb})] v_r^2 = n_0 - 2. \quad (2.27b)$$

The number of gap equations which should be solved is equal to the dimension of the configuration space for two quasiparticles (all allowed values of  $j_a$ ,  $j_b$ , and  $J$ ). Akkermans, Allaart, and Boeker<sup>6</sup> have adopted the simplifying criterion of neglecting the quasiparticle residual interaction [which means ignoring the last two terms in (2.27a)]. In this way the number of gap equations is drastically reduced, so as to depend only on the allowed single-particle states  $j_a$  and  $j_b$ .

In the present work a similar approximation is made, but one which follows from a different criterion. It can be noted that gap equations (2.24) and (2.25) yield the same results for the SDI and the pairing force, except for the self-energy term  $\mu_s$ , which is equal to

$$\mu_s = G v_s^2 \quad (2.28a)$$

for the pairing force, and to

$$\mu_s = \frac{G}{2} \sum_r \hat{r}^2 v_r^2 \quad (2.28b)$$

for SDI. Realizing, furthermore, that for the pairing force equation (2.27a) reduces to

$$[2u_s v_s (\epsilon_s - \mu_s - \lambda) - (u_s^2 - v_s^2) (\Delta_s - G u_a v_a - G u_b v_b)] [1 - 2\hat{s}^{-2} (\delta_{as} + \delta_{bs})] - 2G u_s v_s (u_s^2 - v_s^2) \delta_{J0} \delta_{as} \delta_{bs} = 0, \quad (2.29)$$

it seems reasonable to work with this simplified equation in place of (2.27a). It should be noted, however, that Eq. (2.29) is identically satisfied for all values of  $u_{3/2}$  and  $v_{3/2}$  when  $J=0$ . Thus, in this case we are obliged to use the unblocked pairing parameters. There is, in principle, no problem in solving the gap equations for the remaining seniority-zero two-quasiparticle states. However, bearing in mind that the seniority-zero states are not orthogonal to each other after the effects of blocking are taken into account<sup>7</sup> (this is what makes the BCS formalism complicated), we decided to use for all seniority-zero two-quasiparticle states the unblocked pairing parameters. With this procedure the basis is now orthogonal and the spurious states are removed following the same technique which is used in BCS approach. It is worth mentioning that, in general, the number of configurations with seniority zero is very small in comparison with the number of states with seniority two.

For the 3qp states we adopt the same approximations discussed before for the 2qp states. Therefore, the gap equations for three quasiparticles blocked in the states  $|\alpha\rangle$ ,  $|\beta\rangle$ , and  $|\gamma\rangle$ ,  $(|\eta\rangle = [(ab)J, c]IM; z=1\rangle)$ , leads to

$$\{2u_s v_s (\epsilon_s - \mu_s - \lambda) - (u_s^2 - v_s^2) [\Delta_s - G(u_a v_a + u_b v_b + u_c v_c)]\} \left[ 1 - \frac{2}{\hat{s}^2} (\delta_{sa} + \delta_{sb} + \delta_{sc}) \right] = 0, \quad (2.30a)$$

$$\sum_s [\hat{s}^2 - 2(\delta_{sa} + \delta_{sb} + \delta_{sc})] v_s^2 = n_0 - 3. \quad (2.30b)$$

TABLE I. Dimensions for some negative parity states of Ni isotopes using the CSM and LSSM approaches. For the various BCS calculations the dimensions for all isotopes are equal to the numbers given in the second column. See text for details.

Spin	<sup>59,65</sup> Ni		<sup>61,63</sup> Ni	
	CSM-BCS	CSM	CSM	LSSM
$\frac{1}{2}$	5	15		10
$\frac{3}{2}$	10	24		18
$\frac{5}{2}$	10	29		20
$\frac{7}{2}$	6	23		14
$\frac{9}{2}$	5	17		11
$\frac{11}{2}$	1	8		3

### III. NUMERICAL CALCULATIONS

We restrict ourselves to single closed-shell nuclei where only an odd number of total nucleons in the open subshells are allowed. For this study we consider examples from the Ni ( $Z=28$ ) isotopes and  $N=82$  isotones. In the first case, we investigate nuclei with 3, 5, 7, and 9 active neutrons occupying the subshells  $2p_{3/2}$ ,  $1f_{5/2}$ , and  $2p_{1/2}$ . Therefore, only negative-parity states will be considered. In the second case we investigate nuclei with 3, 5, 7, 9, and 11 active protons occupying the subshells  $2d_{5/2}$ ,  $1g_{7/2}$ ,  $3s_{1/2}$ , and  $2d_{3/2}$ . We calculate the structure of the low-lying states (level schemes, eigenvectors, electromagnetic moments, and transition rates) using the different approaches CSM, LSSM, BCS, BBCS, and PBCS, which were explained in Secs. I and II.

In Tables I and II we note the dimensions of the configuration spaces we use for the  $Z=28$  isotopes and  $N=82$  isotones, respectively. The dimensions for all three BCS approximations and for all nuclei are given by the numbers in the second columns of these tables. For further discussion it is convenient to introduce here the label  $N_{qp}$  which specifies the number of quasiparticles. Thus, the difference in the number of configurations between the BCS approach and LSSM approach comes from the configurations with  $\nu \leq 3$  and  $N_{qp} \geq 5$ . It is clear that the maximum value of  $N_{qp}$  is equal to the number of

valence particles or holes.

For the  $N=82$  isotones we do not consider the  $1h_{11/2}$  orbital as its inclusion would make the dimensions of the state vectors (for CSM and LSSM) too large for our computational techniques. It is evident that in such a situation the utilization of approximations is essential.

For all five approximations (CSM, LSSM, BCS, BBCS, and PBCS) the Hamiltonians which were diagonalized were based on the following set of parameters.

The single-particle energies  $\epsilon(lj)$  for all Ni isotopes were extracted from experimental results for the <sup>57</sup>Ni nucleus, with the results 0, 0.76, and 1.08 MeV for the orbitals  $p_{3/2}$ ,  $f_{5/2}$ , and  $p_{1/2}$ , respectively. For all odd  $N=82$  isotones the single-particle energies were taken to be 0.0, 0.80, 2.62, and 2.68 MeV for the orbitals  $g_{7/2}$ ,  $d_{5/2}$ ,  $d_{3/2}$ , and  $s_{1/2}$ , respectively, as given in Ref. 14.

For the residual interaction between the valence particles we used the surface delta interaction with strengths

$$G = 0.48 \text{ MeV (Ni isotopes) ,}$$

$$G = 0.20 \text{ MeV (} N = 82 \text{ isotones) ,}$$

which follows from the estimate of Kisslinger and Sorensen.<sup>15</sup>

The energy spectra of Ni isotopes are shown in Figs. 1–4 and the wave functions of a few low-lying states in <sup>61</sup>Ni and <sup>63</sup>Ni are listed in Table III. The seniority structure of these states is presented in Tables IV and V.

In Figs. 5–9 the energy spectra of  $N=82$  isotones from <sup>135</sup>I to <sup>143</sup>Pm are exhibited, while comparisons of the wave functions obtained within the different BCS approximations are presented in Table VI. The seniority composition of the <sup>137</sup>Cs wave functions is presented in Table VII.

The calculations of the magnetic dipole moments  $\mu$  and the  $B(M1)$  values were performed with the following gyromagnetic ratios: (1)  $g_l=0$  and  $g_s^{\text{eff}}=0.7g_s^{\text{free}}$  for Ni isotopes, and (2)  $g_l=1$  and  $g_s^{\text{eff}}=0.4g_s^{\text{free}}$  for  $N=82$  isotones. The electric quadrupole moments  $Q$  and the  $B(E2)$  values were evaluated with the following effective electric charges: (1)  $e_n^{\text{eff}}=1.7e$  for Ni isotopes,<sup>16</sup> and (2)  $e_p^{\text{eff}}=2e$  for  $N=82$  isotones. The results for the electromagnetic properties of Ni and  $N=82$  nuclei are presented in Figs. 10–13 and 14–16, respectively.

TABLE II. Dimensions for some positive parity states of  $N=82$  isotones. See the caption to Table I.

Spin	<sup>135</sup> I		<sup>137</sup> Cs		<sup>139</sup> La		<sup>141</sup> Pr and <sup>143</sup> Pm	
	CSM-BCS	CSM	LSSM	CSM	LSSM	CSM	LSSM	
$\frac{1}{2}$	12	107	39	415	73	790	96	
$\frac{3}{2}$	25	198	80	764	149	1484	198	
$\frac{5}{2}$	28	253	93	1005	174	1965	231	
$\frac{7}{2}$	27	271	91	1121	173	2215	231	
$\frac{9}{2}$	23	252	82	1091	159	2214	215	
$\frac{11}{2}$	16	211	59	974	117	2017	160	
$\frac{13}{2}$	8	153	30	783	62	1669	86	
$\frac{15}{2}$	5	105	20	577	41	1284	57	

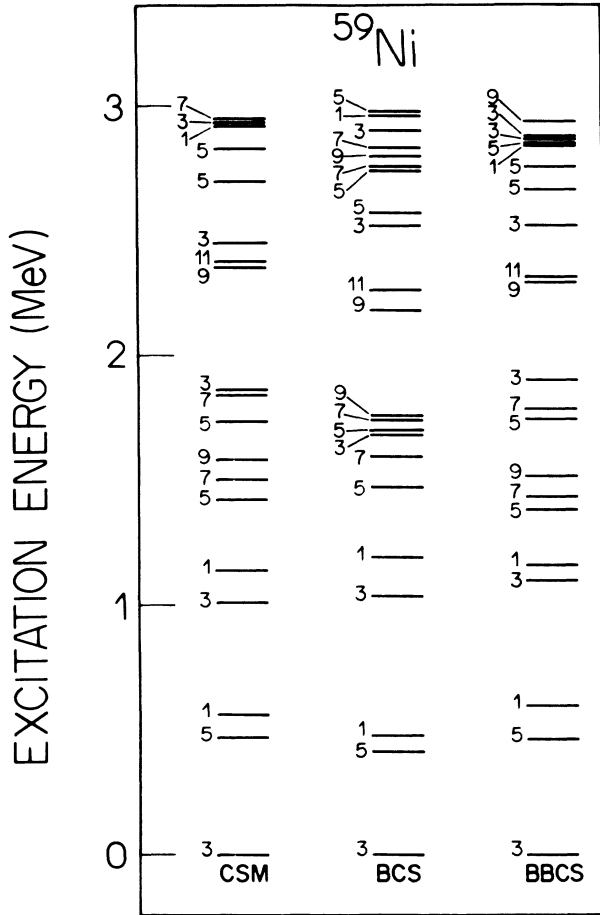


FIG. 1. Calculated energy levels for the negative-parity states in <sup>59</sup>Ni obtained with the different model approaches (see text for details). The spins  $J$  are listed as  $2J$ . In this case the CSM, LSSM, and PBCS results are identical.

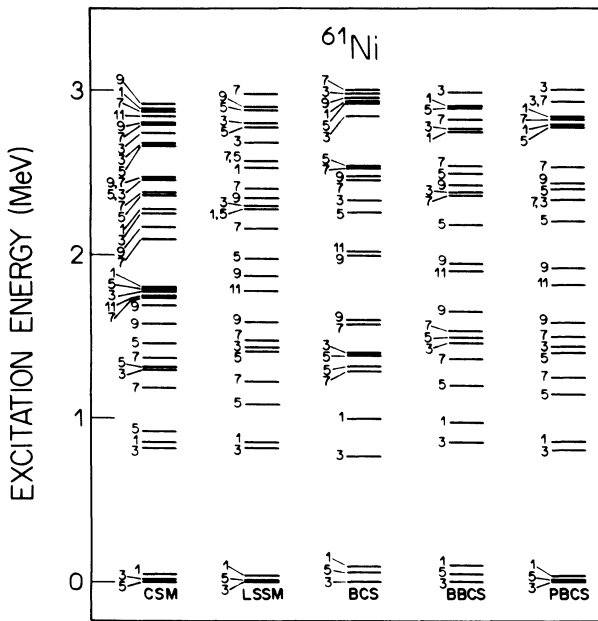


FIG. 2. Calculated energy levels of <sup>61</sup>Ni. The presentation is described in the caption to Fig. 1.

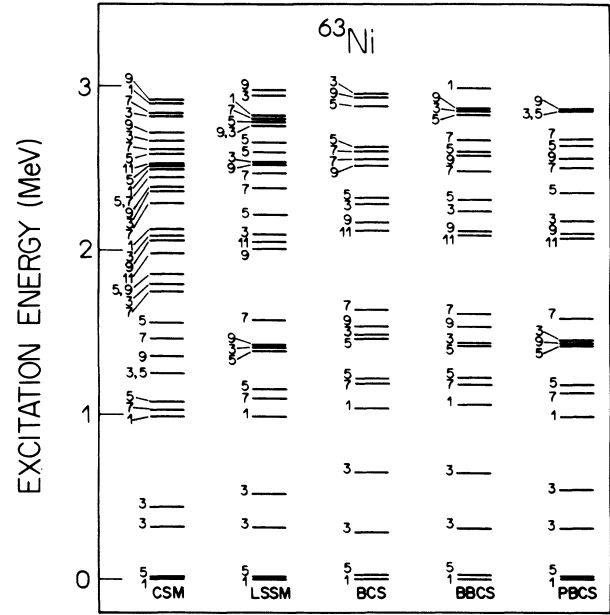


FIG. 3. Calculated energy levels of <sup>63</sup>Ni.

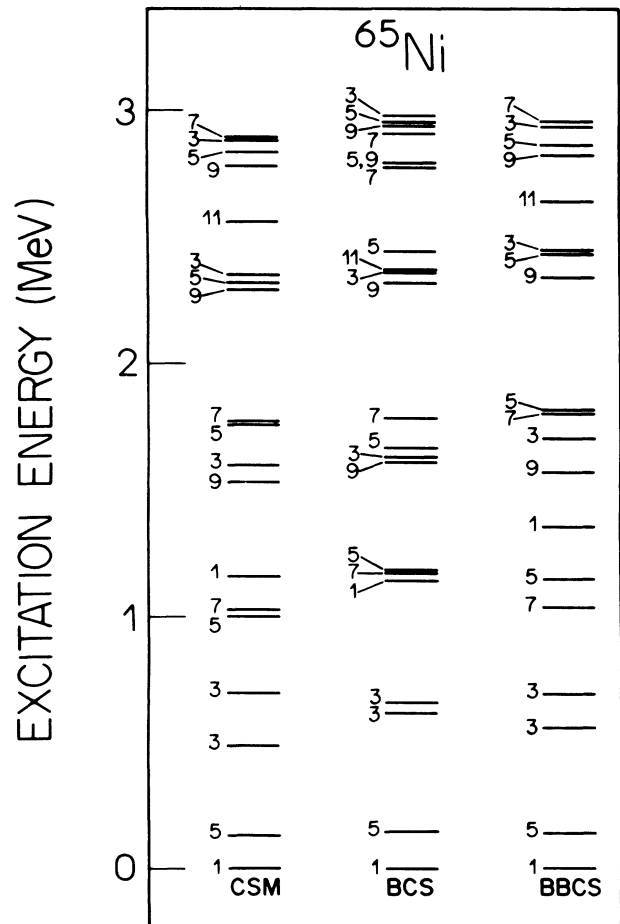


FIG. 4. Calculated energy levels of <sup>65</sup>Ni.

IV. DISCUSSION

A. Effects of configurations with  $\nu=5$  on the low-lying states

In order to evaluate the degree to which configurations with  $\nu=5$  participate in the structure of low-lying states,

we compare the results obtained within the LSSM approximation with the CSM results. We first analyze  $^{61}\text{Ni}$  and  $^{63}\text{Ni}$  (within the single-particle subspace considered in the present work the states of  $^{59}\text{Ni}$  and  $^{65}\text{Ni}$  have only  $\nu=1$  and  $\nu=3$  configurations even in the CSM space). From Figs. 2 and 3 we can see that the LSSM energy

TABLE III. Calculated wave functions of some low-lying states in  $^{61,63}\text{Ni}$  using different BCS approaches. The basis states are  $|(j_a j_b) J, J_c, J_i\rangle$ . Only amplitudes larger than 4% are listed.

$J_i$	$j_a$	$j_b$	$J_{ab}$	$J_c$	$^{61}\text{Ni}$			$^{63}\text{Ni}$		
					BCS	BBCS	PBCS	BCS	BBCS	PBCS
$\frac{3}{2}_1$				$\frac{3}{2}$	0.960	0.961	0.968	0.953	0.961	0.956
$\frac{5}{2}_1$				$\frac{5}{2}$	0.981	0.979	0.984	0.987	0.986	0.992
$\frac{1}{2}_1$				$\frac{1}{2}$	0.890	0.895	0.834	0.941	0.940	0.948
	$\frac{3}{2}$	$\frac{3}{2}$	0	$\frac{1}{2}$						
	$\frac{3}{2}$	$\frac{3}{2}$	2	$\frac{5}{2}$	0.203	0.196	0.208			
	$\frac{3}{2}$	$\frac{1}{2}$	2	$\frac{5}{2}$	-0.276	-0.265	-0.295			
	$\frac{5}{2}$	$\frac{5}{2}$	2	$\frac{3}{2}$	0.226	0.224	0.250			
$\frac{3}{2}_2$				$\frac{3}{2}$	0.198	0.224	0.206			0.214
	$\frac{3}{2}$	$\frac{3}{2}$	0	$\frac{3}{2}$	0.194	0.257	0.268			
	$\frac{5}{2}$	$\frac{5}{2}$	2	$\frac{1}{2}$	0.528	0.416	0.411	0.634	0.633	0.620
	$\frac{3}{2}$	$\frac{3}{2}$	2	$\frac{5}{2}$	-0.317	-0.340	-0.340	-0.240	-0.217	-0.218
	$\frac{3}{2}$	$\frac{1}{2}$	2	$\frac{5}{2}$	0.483	0.559	0.579	0.397	0.396	0.384
	$\frac{5}{2}$	$\frac{5}{2}$	2	$\frac{5}{2}$	0.517	0.443	0.439	0.563	0.586	0.594
$\frac{1}{2}_2$				$\frac{1}{2}$	-0.455	-0.446	-0.463	0.338	0.341	0.316
	$\frac{3}{2}$	$\frac{3}{2}$	0	$\frac{1}{2}$	-0.306	-0.306	-0.435	0.344	0.353	0.432
	$\frac{5}{2}$	$\frac{5}{2}$	0	$\frac{1}{2}$	0.254	0.276		0.231	0.242	
	$\frac{5}{2}$	$\frac{5}{2}$	2	$\frac{3}{2}$	0.444	0.463	0.451	-0.473	-0.465	-0.473
	$\frac{3}{2}$	$\frac{3}{2}$	2	$\frac{5}{2}$	0.407	0.397	0.368	-0.377	-0.345	-0.345
	$\frac{3}{2}$	$\frac{1}{2}$	2	$\frac{5}{2}$	-0.522	-0.510	-0.508	0.590	0.604	0.609
$\frac{5}{2}_2$				$\frac{5}{2}$				0.353	0.328	0.462
	$\frac{1}{2}$	$\frac{1}{2}$	0	$\frac{5}{2}$						
	$\frac{3}{2}$	$\frac{3}{2}$	0	$\frac{5}{2}$	0.268	0.220	0.361			
	$\frac{5}{2}$	$\frac{5}{2}$	0	$\frac{5}{2}$	-0.305	-0.201		-0.343	-0.338	
	$\frac{3}{2}$	$\frac{5}{2}$	2	$\frac{5}{2}$	-0.557	-0.478	-0.472			
	$\frac{5}{2}$	$\frac{5}{2}$	2	$\frac{3}{2}$	0.419	0.556	0.547			
	$\frac{3}{2}$	$\frac{3}{2}$	2	$\frac{1}{2}$	0.398	0.489	0.466			
	$\frac{5}{2}$	$\frac{5}{2}$	2	$\frac{1}{2}$	-0.221			-0.609	-0.584	-0.615
	$\frac{3}{2}$	$\frac{1}{2}$	1	$\frac{5}{2}$	0.231	0.307	0.288			
	$\frac{3}{2}$	$\frac{1}{2}$	2	$\frac{5}{2}$				-0.512	-0.572	-0.540
	$\frac{5}{2}$	$\frac{5}{2}$	4	$\frac{3}{2}$				0.240	0.227	0.240
	$\frac{3}{2}$	$\frac{3}{2}$	2	$\frac{5}{2}$				0.216		
$\frac{7}{2}_1$				$\frac{3}{2}$						
	$\frac{5}{2}$	$\frac{5}{2}$	2	$\frac{3}{2}$	0.418	0.630	0.624	0.328	0.362	0.346
	$\frac{3}{2}$	$\frac{1}{2}$	2	$\frac{5}{2}$	0.453	0.525	0.520	0.418	0.444	0.437
	$\frac{3}{2}$	$\frac{3}{2}$	4	$\frac{1}{2}$	0.629	0.399	0.385			
	$\frac{5}{2}$	$\frac{5}{2}$	4	$\frac{3}{2}$	0.312	0.222	0.272	0.266	0.250	0.261
	$\frac{3}{2}$	$\frac{3}{2}$	2	$\frac{5}{2}$	-0.341			-0.255	-0.200	-0.217
	$\frac{3}{2}$	$\frac{1}{2}$	1	$\frac{5}{2}$		-0.313	-0.306			
	$\frac{5}{2}$	$\frac{5}{2}$	4	$\frac{1}{2}$				0.761	0.750	0.755

TABLE IV. Seniority ( $\nu$ ) decompositions in percent (%) and the values of the average seniority for wave functions of selected states in  $^{61}\text{Ni}$  obtained with the CSM and LSSM approaches.

Spin	$\nu=1$ (%)		$\nu=3$ (%)		$\nu=5$ (%)		$\bar{\nu}$	
	CSM	LSSM	CSM	LSSM	CSM	CSM	LSSM	
$\frac{5}{2}_1$	95.58	97.01	3.66	2.99	0.76	1.10	1.06	
$\frac{3}{2}_1$	93.80	94.01	6.15	5.99	0.05	1.12	1.12	
$\frac{1}{2}_1$	79.89	80.47	19.84	19.53	0.27	1.41	1.39	
$\frac{3}{2}_2$	10.90	11.86	88.67	88.14	0.43	2.78	2.76	
$\frac{1}{2}_2$	42.57	40.80	56.53	59.20	0.90	2.17	2.18	
$\frac{5}{2}_2$	15.81	14.62	72.96	85.38	11.23	2.91	2.71	
$\frac{7}{2}_1$	0	0	94.90	100	5.10	3.10	3	
$\frac{3}{2}_3$	18.84	18.33	60.92	81.67	20.24	3.03	2.63	
$\frac{5}{2}_3$	23.68	15.96	52.65	84.04	23.67	2.99	2.68	
$\frac{7}{2}_2$	0	0	91.86	100	8.14	3.16	3	
$\frac{5}{2}_4$	11.59		80.73		7.68	2.94		
$\frac{9}{2}_1$	0	0	98.69	100	1.31	3.03	3	
$\frac{9}{2}_2$	0	0	84.03	100	15.97	3.32	3	
$\frac{7}{2}_3$	0		68.21		31.79	3.64		
$\frac{11}{2}_1$	0	0	97.68	100	2.32	3.05	3	
$\frac{3}{2}_4$	6.34		46.51		47.15	3.83		
$\frac{1}{2}_3$	11.60		57.40		31.00	3.40		
$\frac{5}{2}_5$	8.84		53.63		37.53	3.46		

spectra are less compressed than are those of the CSM. However, the numbers of states lying within the first 3 MeV of excitation energy are not very different in these two models; there are 29 and 28 states for  $^{61}\text{Ni}$  and  $^{63}\text{Ni}$ , respectively, in the LSSM spectra while the corresponding numbers in the CSM spectra are 37 and 35.

In Tables IV and V the seniority structure and the mean values of the mean values of the seniority  $\bar{\nu}$  for several low-lying states in  $^{61}\text{Ni}$  and  $^{63}\text{Ni}$ , respectively, are presented. In both models the  $\frac{1}{2}_1^-$ ,  $\frac{3}{2}_1^-$ , and  $\frac{5}{2}_1^-$  levels have predominant  $\nu=1$  character. The remaining levels are dominated by  $\nu=3$  configurations. As expected, the

TABLE V. Seniority structure of wave functions of  $^{63}\text{Ni}$ , as described in the caption to Table IV.

Spin	$\nu=1$ (%)		$\nu=3$ (%)		$\nu=5$ (%)		$\bar{\nu}$	
	CSM	LSSM	CSM	LSSM	CSM	CSM	LSSM	
$\frac{1}{2}_1$	90.46	90.65	9.49	9.35	0.05	1.19	1.19	
$\frac{5}{2}_1$	98.09	98.43	1.77	1.57	0.14	1.04	1.03	
$\frac{3}{2}_1$	89.30	91.20	10.68	8.80	0.02	1.21	1.18	
$\frac{3}{2}_2$	8.04	6.88	88.07	93.12	3.89	2.92	2.86	
$\frac{1}{2}_2$	29.14	28.76	70.44	71.24	0.42	2.43	2.43	
$\frac{7}{2}_1$	0	0	94.45	100	5.55	3.11	3	
$\frac{5}{2}_2$	24.14	23.41	66.46	76.59	9.40	2.71	2.53	
$\frac{3}{2}_3$	13.72	17.50	71.84	82.50	14.44	3.01	2.65	
$\frac{5}{2}_3$	6.80	8.11	80.51	91.89	12.69	3.12	2.84	
$\frac{9}{2}_1$	0	0	94.43	100	5.57	3.11	3	
$\frac{7}{2}_2$	0	0	87.15	100	12.85	3.26	3	
$\frac{5}{2}_4$	21.53		45.94		32.53	3.22		
$\frac{7}{2}_3$	0		72.23	100	27.77	3.56		
$\frac{3}{2}_4$	9.89		66.54		23.57	3.28		
$\frac{9}{2}_2$	0	0	86.14	100	13.86	3.28	3	
$\frac{5}{2}_5$	3.99		54.49		41.52	3.75		

values of  $\bar{\nu}$  increase with excitation energy. It should also be noted that for a given total angular momentum  $J$  the mean seniority of the state  $J_n$  is always smaller than that of the state  $J_{n+1}$  and that the influence of configurations with  $\nu=5$  commence to be pronounced for levels with  $n=3$ .

We discuss the electromagnetic properties of  $^{59}\text{Ni}$ ,  $^{61}\text{Ni}$ ,  $^{63}\text{Ni}$ , and  $^{65}\text{Ni}$  in the following order: (i) the states with  $\bar{\nu}\approx 1$ , i.e., the levels  $\frac{1}{2}^-$ ,  $\frac{3}{2}^-$ , and  $\frac{5}{2}^-$  (with a fraction of  $\nu=5$  configurations smaller than 1%); (ii) the levels  $\frac{7}{2}^-$ ,  $\frac{9}{2}^-$ ,  $\frac{1}{2}^-$ ,  $\frac{3}{2}^-$ , and  $\frac{5}{2}^-$ , for which  $\bar{\nu}\approx 3$  and the admixtures of  $\nu=5$  configurations range between 1% and 11%;

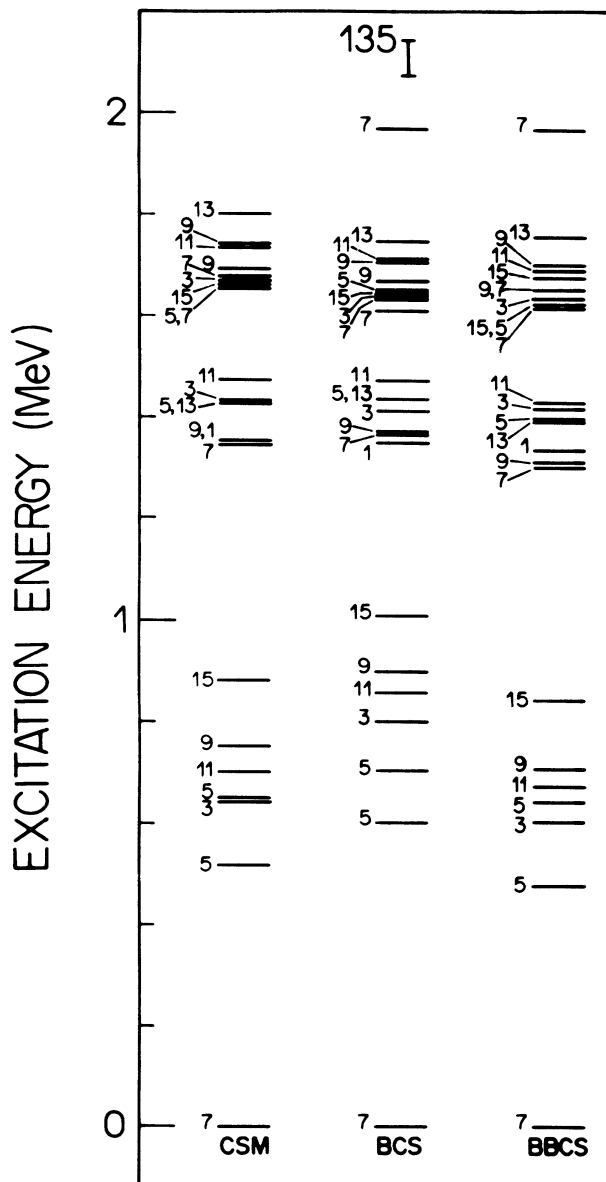


FIG. 5. Calculated energy levels for the positive-parity states of  $^{135}\text{I}$  obtained with different model approaches (see text for details). The spins  $J$  are listed as  $2J$ . In this case the results with CSM, LSSM, and PBCS are identical.

and (iii) a few selected additional levels ( $\frac{7}{2}^-$ ,  $\frac{3}{2}^-$ , and  $\frac{5}{2}^-$ ), in which  $\bar{\nu}\approx 3$  and in which the fraction of  $\nu=5$  configurations varies from 8% to 24%.

The results for the magnetic dipole and electric quadrupole moments are presented as a function of the mass number in Figs. 10 and 11, respectively. As might be anticipated the LSSM results are very similar to the CSM calculations for all three levels with  $\bar{\nu}\approx 1$ . For the second group of states, i.e., the lowest states with  $\bar{\nu}\approx 3$ , the differences between the LSSM and the CSM results are significant. The only exception are the values of the magnetic moments of the  $\frac{1}{2}^-$  state. The differences between the two calculations of the electromagnetic moments are still more accentuated for levels which belong to the third group of states.

The  $B(M1)$  and  $B(E2)$  values for Ni isotopes, displayed in Figs. 12 and 13, respectively, always have as the final state one of the levels  $\frac{1}{2}^-$ ,  $\frac{3}{2}^-$ , or  $\frac{5}{2}^-$ . One immediately sees that when the transition is initiated in one of the levels  $\frac{1}{2}^-$ ,  $\frac{3}{2}^-$ ,  $\frac{5}{2}^-$ ,  $\frac{7}{2}^-$ ,  $\frac{9}{2}^-$ ,  $\frac{1}{2}^-$ , and  $\frac{3}{2}^-$ , which contain relatively small amounts  $\nu=5$  configurations, the LSSM and the CSM calculations yield similar results. Moreover, the differences between these calculations are also small for the  $B(M1)$  values in which the initial states are  $\frac{7}{2}^-$  and  $\frac{5}{2}^-$ , and for the  $B(E2)$  values in which the initial states are  $\frac{7}{2}^-$ ,  $\frac{3}{2}^-$ , and  $\frac{5}{2}^-$ . In other transitions the deviations of the LSSM results from the CSM values are

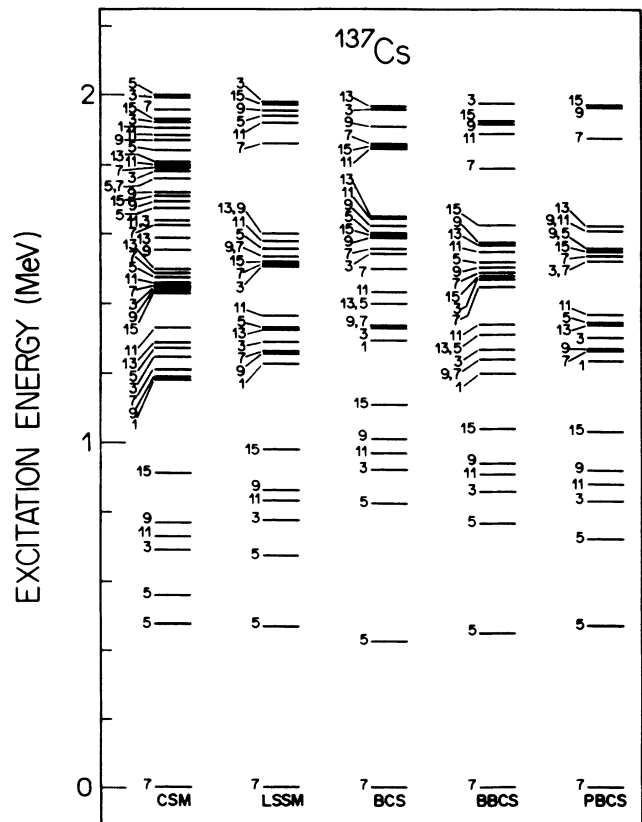


FIG. 6. Calculated energy levels of  $^{137}\text{Cs}$ .

quite important.

As a supplement to the study of the Ni isotopes we next compare the LSSM and CSM descriptions of  $^{137}\text{Cs}$ . From the results shown in Fig. 6 one observes that up to 1.4 MeV in excitation energy the LSSM level scheme is very similar to the corresponding CSM spectrum. Both spectra exhibit the same number of states, the energy differences are very small ( $\lesssim 120$  keV), and, except for the inversion of the  $\frac{11}{2}^+$  and  $\frac{5}{2}^+$  states, the ordering of the levels is also the same. For the states compressed in the energy interval between 1.4 and 1.6 MeV, the energy differences are relatively small, but the ordering of the levels is different and the density of states is slightly smaller within the LSSM. Above 1.6 MeV excitation energy the influence of  $\nu=5$  configurations is quite pronounced and, as a consequence, the level density is significantly diminished in the truncated configuration space.

In Table VII the seniority compositions and the mean seniorities for levels of  $^{137}\text{Cs}$  with excitation energy lower than 1.6 MeV are presented. Only the first two levels in the  $^{137}\text{Cs}$  nucleus have predominantly  $\nu=1$  character, all remaining levels have  $\bar{\nu}\approx 3$ . The fraction of  $\nu=5$

configurations is smaller than 6% for states which lie below 1.4 MeV, between 6% and 10% for levels with excitation energy between 1.4 and 1.6 MeV, and for levels above 1.6 MeV are in most cases larger than 10% with some going up to 50%.

The analysis of the electromagnetic properties of  $^{137}\text{Cs}$  in the LSSM and CSM spaces performed for (i) the states with  $\bar{\nu}\approx 1$ , i.e., the levels  $\frac{5}{2}^+$  and  $\frac{7}{2}^+$ ; (ii) the first states for each spin with  $\bar{\nu}\approx 3$ , i.e., the levels  $\frac{1}{2}^+$ ,  $\frac{3}{2}^+$ ,  $\frac{9}{2}^+$ ,  $\frac{11}{2}^+$ ,  $\frac{13}{2}^+$ ,  $\frac{15}{2}^+$ ,  $\frac{5}{2}^+$ , and  $\frac{7}{2}^+$ ; and (iii) the state  $\frac{3}{2}^+$  which for heavier isotones it turns out to be the lowest  $\bar{\nu}\approx 3$  state with spin and parity  $\frac{3}{2}^+$ .

The LSSM and CSM magnetic-field dipole moments for the levels  $\frac{1}{2}^+$ ,  $\frac{3}{2}^+$ ,  $\frac{5}{2}^+$ ,  $\frac{7}{2}^+$ ,  $\frac{9}{2}^+$ ,  $\frac{11}{2}^+$ ,  $\frac{13}{2}^+$ ,  $\frac{15}{2}^+$ ,  $\frac{3}{2}^+$ ,  $\frac{5}{2}^+$ , and  $\frac{7}{2}^+$ , as well as the  $B(M1)$  values for the transitions  $\frac{9}{2}^+ \rightarrow \frac{11}{2}^+$  and  $\frac{13}{2}^+ \rightarrow \frac{11}{2}^+$  are compared in Fig. 14. Except for the last transitions, the LSSM and the CSM lead to almost identical results for all these observables. We do not present here the results for the remaining  $M1$  transitions which take place among the above-mentioned states. It is due to the fact that, as a consequence of the  $l$  forbiddenness, they are all very weak (smaller than  $10^{-3}$

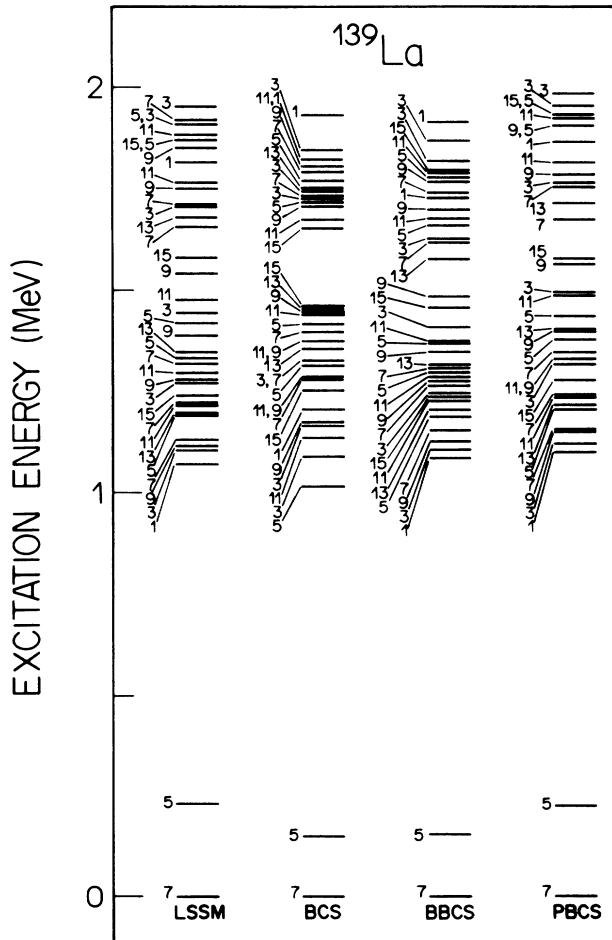


FIG. 7. Calculated energy levels of  $^{139}\text{La}$ .

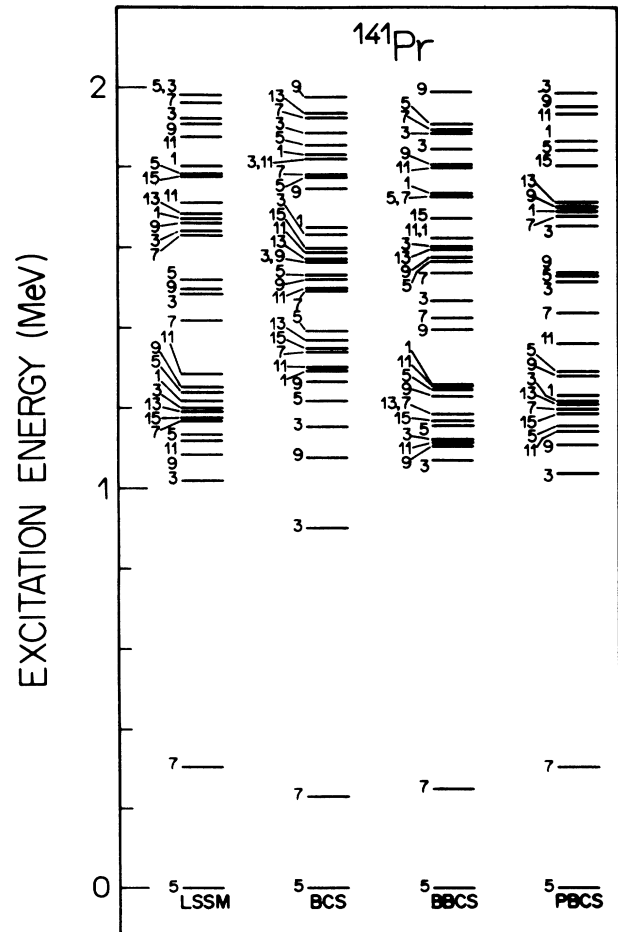


FIG. 8. Calculated energy levels of  $^{141}\text{Pr}$ .



TABLE VI. (Continued).

$I_i$	$^{137}\text{Cs}$				$^{139}\text{La}$				$^{141}\text{Pr}$				$^{143}\text{Pm}$					
	$j_a$	$j_b$	$J_{ab}$	$j_c$	BCS	PBCS	BCS	BBCS	PBCS	BCS	BBCS	PBCS	BCS	BBCS	PBCS	BCS	BBCS	PBCS
$\frac{1}{2}^-$	$\frac{7}{2}^-$	$\frac{7}{2}^-$	0	$\frac{7}{2}^-$	-0.467	-0.321												
	$\frac{5}{2}^-$	$\frac{5}{2}^-$	0	$\frac{5}{2}^-$	0.528													
	$\frac{7}{2}^-$	$\frac{7}{2}^-$	2	$\frac{5}{2}^-$	0.643	0.927												
	$\frac{5}{2}^-$	$\frac{5}{2}^-$	2	$\frac{7}{2}^-$	0.959	0.969	0.944											
	$\frac{7}{2}^-$	$\frac{7}{2}^-$	4	$\frac{5}{2}^-$	0.968													
	$\frac{5}{2}^-$	$\frac{5}{2}^-$	4	$\frac{7}{2}^-$	0.959													
$\frac{5}{2}^-$	$\frac{7}{2}^-$	$\frac{7}{2}^-$	0	$\frac{7}{2}^-$	-0.290													
	$\frac{5}{2}^-$	$\frac{5}{2}^-$	0	$\frac{5}{2}^-$	0.468	0.267												
	$\frac{7}{2}^-$	$\frac{7}{2}^-$	2	$\frac{5}{2}^-$	-0.742	-0.730												
	$\frac{5}{2}^-$	$\frac{5}{2}^-$	2	$\frac{7}{2}^-$	0.232	0.349	0.279											
	$\frac{7}{2}^-$	$\frac{7}{2}^-$	4	$\frac{7}{2}^-$	0.953	0.971	0.279											
	$\frac{5}{2}^-$	$\frac{5}{2}^-$	4	$\frac{5}{2}^-$	0.953		0.361	0.397										

W.u.) and therefore the tensor  $M1$  operator  $[Y_2 \otimes \sigma]_1$ , not considered in the present work, plays an important role.

From the results, for the electric quadrupole moments of the low-lying states in  $^{137}\text{Cs}$ , shown in Fig. 15, we can see that the effect of configurations with  $\nu=5$  on these observables is negligibly small for the levels  $\frac{7}{2}^+$ ,  $\frac{9}{2}^+$ ,  $\frac{11}{2}^+$ , and  $\frac{3}{2}^+$ . The differences between the LSSM and CSM results for the remaining six states, although relatively small, are significant. It is worthwhile to notice that in the case of the  $\frac{5}{2}^+$  and  $\frac{5}{2}^+$  levels these differences arise both (1) from the rearrangement of the  $\nu=1$  and  $\nu=3$  amplitudes in the corresponding wave functions, induced by the  $\nu=5$  configurations (see Table VII) and (2) from the destructive interference between the  $\nu=1$  and  $\nu=3$  contributions on the quadrupole moments  $Q(\frac{5}{2}^+)$  and  $Q(\frac{5}{2}^+)$ .

The results for the  $B(E2)$  values, exhibited in Fig. 16, clearly demonstrate that relatively small admixture of  $\nu=5$  configurations in the low-lying states affect the magnitudes of the  $\frac{5}{2}^+ \rightarrow \frac{7}{2}^+$ ,  $\frac{5}{2}^+ \rightarrow \frac{7}{2}^+$ ,  $\frac{9}{2}^+ \rightarrow \frac{11}{2}^+$ , and  $\frac{15}{2}^+ \rightarrow \frac{11}{2}^+$  electric transitions to a great extent. In the first two processes, the modifications are caused by the

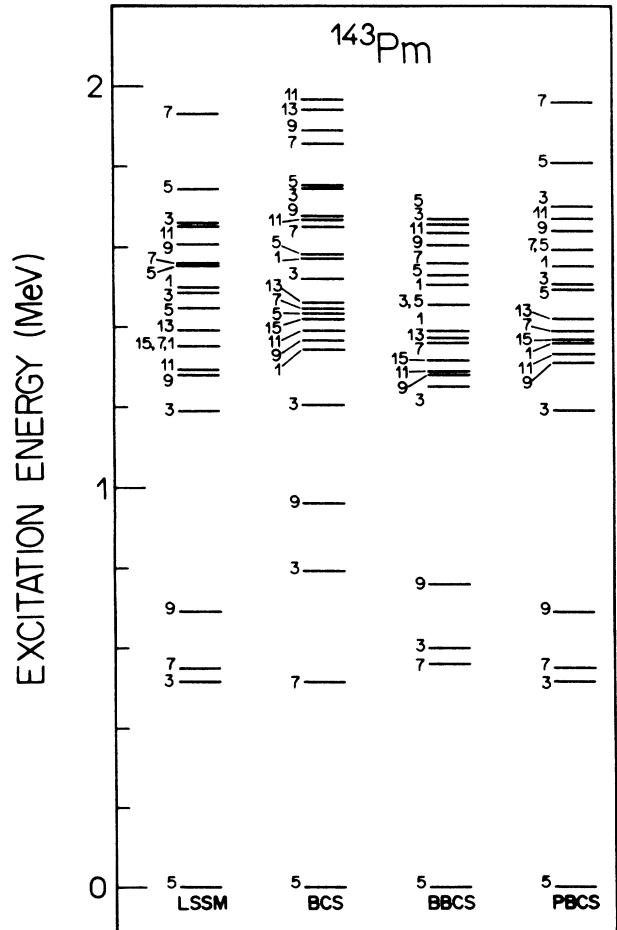


FIG. 9. Calculated energy levels of  $^{143}\text{Pm}$ .

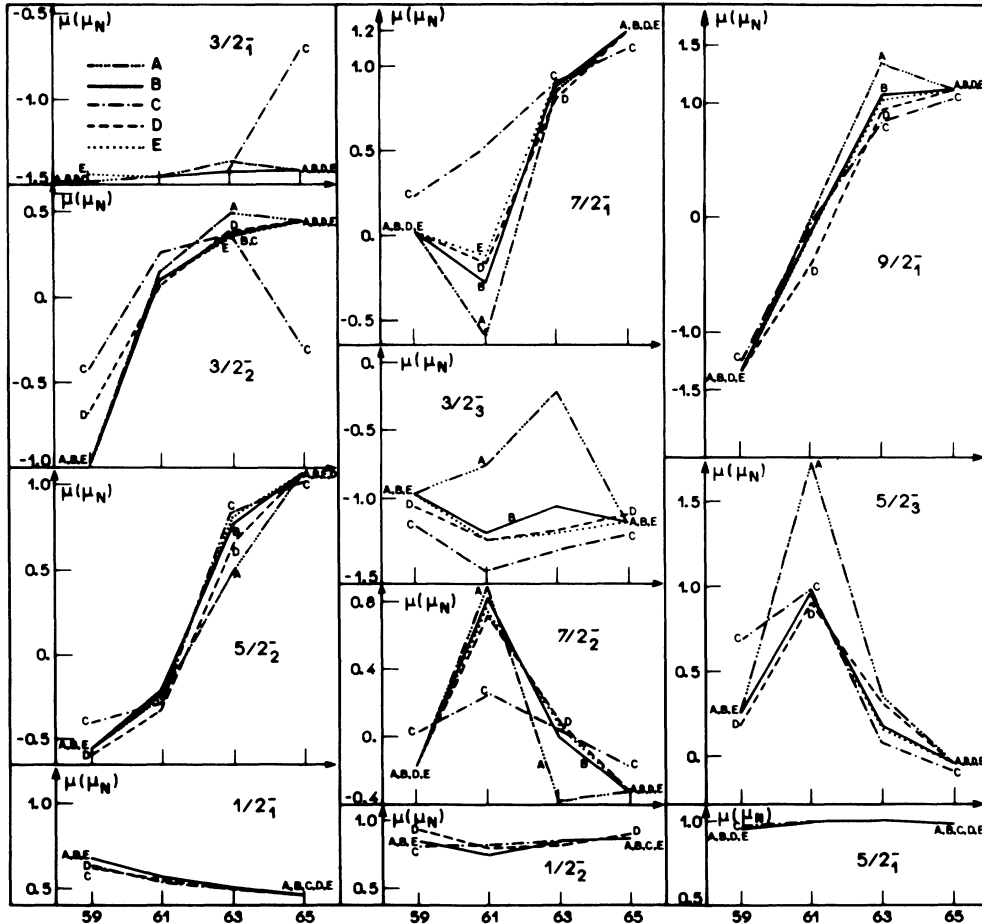


FIG. 10. Calculated magnetic dipole moments in units of nuclear magnetons (n.m.) for some low-lying levels of the Ni isotopes as a function of the mass number  $A$  ( $59 \leq A \leq 65$ ). The results from the CSM, LSSM, BCS, BBCS, and PBCS approximations are labeled with the letters  $A, B, C, D$ , and  $E$ , respectively.

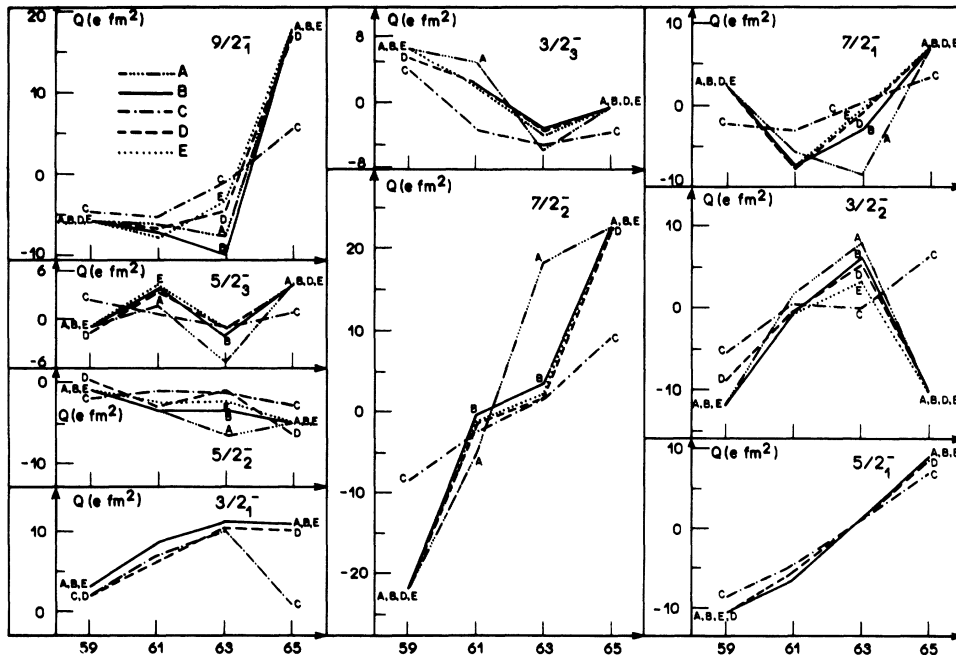
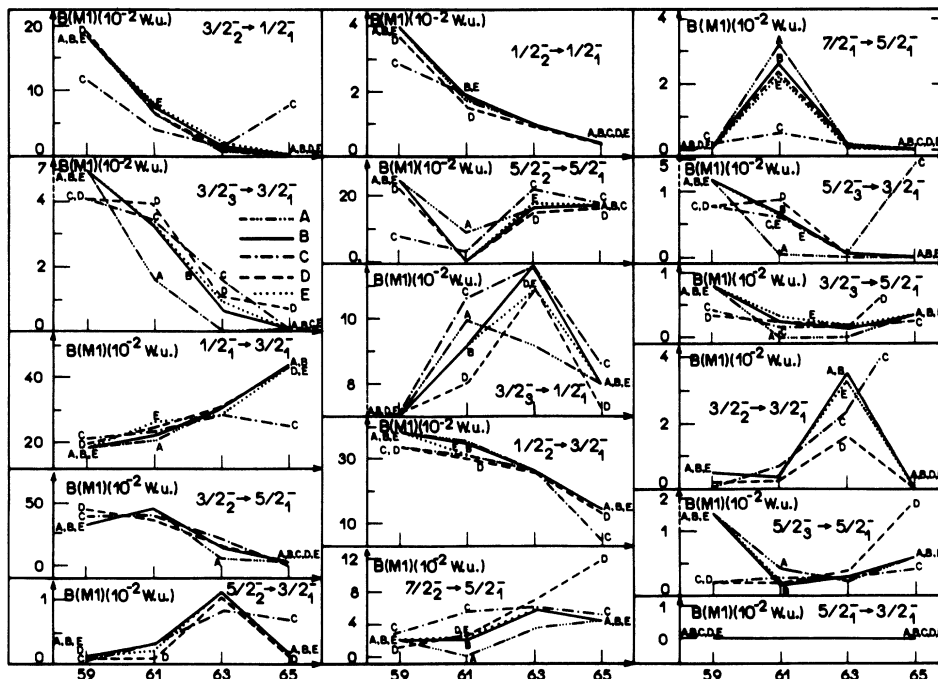


FIG. 11. Calculated electric quadrupole moments in units of  $e \text{ fm}^2$  for some low-lying levels of the Ni isotopes as a function of the mass number  $A$  ( $59 \leq A \leq 65$ ). For further explanation see the caption to Fig. 10.

TABLE VII. Seniority structure of wave functions of  $^{137}\text{Cs}$ . The presentation is as described in the caption to Table IV.

Spin	$\nu=1$ (%)		$\nu=3$ (%)		$\nu=5$ (%)		$\bar{\nu}$	LSSM
	CSM	LSSM	CSM	LSSM	CSM	CSM		
$\frac{7}{2}_1$	97.75	98.22	2.07	1.78	0.18	1.05	1.04	
$\frac{5}{2}_1$	90.48	96.02	9.40	3.98	0.12	1.20	1.08	
$\frac{5}{2}_2$	7.17	2.28	89.17	97.72	3.66	2.96	2.95	
$\frac{3}{2}_1$	0.00	0.00	95.28	100.00	4.72	3.08	3.00	
$\frac{11}{2}_1$			94.00	100.00	6.00	3.11	3.00	
$\frac{9}{2}_1$			93.98	100.00	6.02	3.11	3.00	
$\frac{15}{2}_1$			96.03	100.00	3.97	3.08	3.00	
$\frac{1}{2}_1$	3.07	3.59	93.04	96.41	3.89	3.02	2.93	
$\frac{9}{2}_2$			96.45	100.00	3.55	3.10	3.00	
$\frac{7}{2}_2$	0.60	1.20	94.74	98.80	4.66	3.06	2.98	
$\frac{3}{2}_2$	3.07	3.86	93.63	96.14	3.30	3.03	2.92	
$\frac{5}{2}_2$	1.74	1.50	95.10	98.50	3.16	3.06	2.97	
$\frac{13}{2}_1$			94.99	100.00	5.01	3.10	3.00	
$\frac{11}{2}_2$			97.75	100.00	2.25	3.06	3.00	
$\frac{15}{2}_2$			90.47	100.00	9.53	3.19	3.00	
$\frac{9}{2}_3$			85.14	100.00	14.86	3.33	3.00	
$\frac{3}{2}_3$	1.59	1.73	94.19	98.27	5.81	3.11	2.96	
$\frac{7}{2}_3$	1.15	4.71	97.70	95.29	8.67	3.19	2.91	
$\frac{11}{2}_3$			80.87	100.00	19.13	3.41	3.00	
$\frac{5}{2}_4$	3.17	4.47	86.88	95.53	9.95	3.17	2.91	
$\frac{7}{2}_4$	48.20	41.47	48.79	58.53	3.01	2.13	2.16	
$\frac{13}{2}_2$			54.24	100.00	45.76	3.91	3.00	
$\frac{9}{2}_4$			93.68	100.00	6.32	3.16	3.00	
$\frac{13}{2}_3$			33.51	100.00	66.49	4.32	3.00	

FIG. 12. Calculated  $M1$  transition rates in units of  $10^{-2}$  W.u. for some transitions in the Ni isotope as a function of the mass number  $A$  ( $59 \leq A \leq 65$ ). For further explanation see the caption to Fig. 10.

above mentioned rearrangement of the  $\nu=1$  and  $\nu=3$  configurations in the wave functions of the  $\frac{5}{2}^+$  and  $\frac{5}{2}^+$  states.

### B. Influence of the configurations with seniority $\nu=1$ and $\nu=3$ and $N_{qp} \geq 5$

We compare in this section the results of PBCS approximation with the LSSM results. It is evident that for  $^{59}\text{Ni}$ ,  $^{65}\text{Ni}$ , and  $^{135}\text{I}$  both calculations should lead to identical results but in the cases of  $^{61}\text{Ni}$ ,  $^{63}\text{Ni}$ , and  $^{137}\text{Cs}$  differences can arise from the effects of five-quasiparticle states with  $\nu=1$  and 3. For the heavier  $N=82$  isotones differences can also arise from configurations with  $N_{qp} > 5$  in the LSSM spaces.

From the energy spectra for  $^{61}\text{Ni}$  and  $^{63}\text{Ni}$  shown in Figs. 2 and 3 we can see that the PBCS approximation and the LSSM yield quite similar results up to an excita-

tion energy of 2 MeV. The number of states is the same in both calculations and, except for one inversion in  $^{63}\text{Ni}$ , the ordering of the levels is also the same. The differences in excitation energies are smaller than 70 keV in  $^{61}\text{Ni}$  and smaller than 40 keV in  $^{63}\text{Ni}$ .

The calculations of the electromagnetic properties for the Ni isotopes displayed in Figs. 10–13, show that one obtains identical results within the PBCS and the LSSM approaches for: (1) magnetic dipole moments of the states  $\frac{3}{2}^-$ ,  $\frac{5}{2}^-$ , and  $\frac{7}{2}^-$ ; (2) electric quadrupole moments of the states  $\frac{3}{2}^-$  and  $\frac{5}{2}^-$ ; (3)  $B(M1)$  values for the transitions initiated in the states  $\frac{1}{2}^-$ ,  $\frac{3}{2}^-$ ,  $\frac{5}{2}^-$ ,  $\frac{7}{2}^-$ ,  $\frac{9}{2}^-$ ,  $\frac{1}{2}^-$ ,  $\frac{3}{2}^-$ , and  $\frac{5}{2}^-$ ; and (4)  $B(E2)$  values for the transitions which involve the states  $\frac{1}{2}^-$ ,  $\frac{3}{2}^-$ ,  $\frac{5}{2}^-$ ,  $\frac{7}{2}^-$ ,  $\frac{3}{2}^-$ , and  $\frac{5}{2}^-$ . Moreover, the corresponding differences for the remaining observables analyzed in the present work are of minor importance. For example, the magnetic moments differ by no more than 0.15 n.m. (nuclear magnetons).

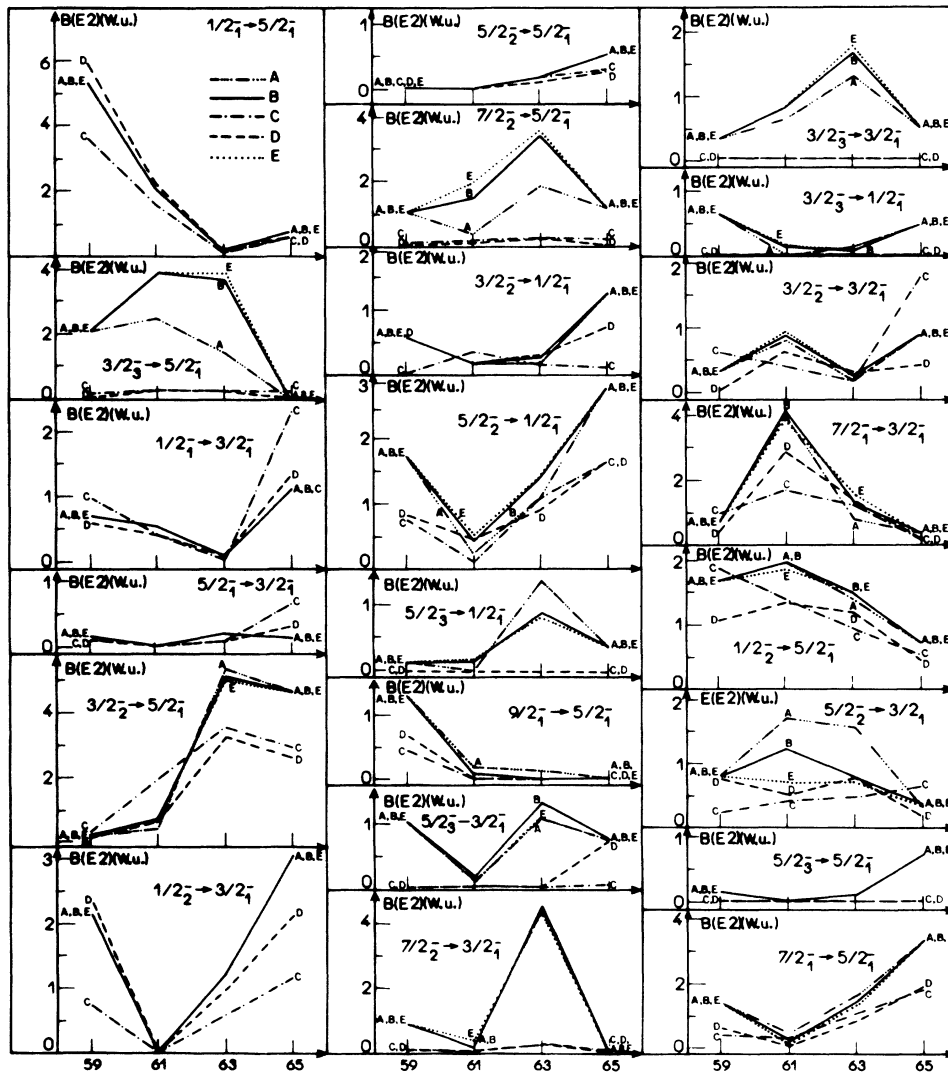


FIG. 13. Calculated  $E2$  transition rates in W.u. units for some transitions in the Ni isotopes as a function of the mass number  $A$  ( $59 \leq A \leq 65$ ). For further explanation see the caption to Fig. 10.

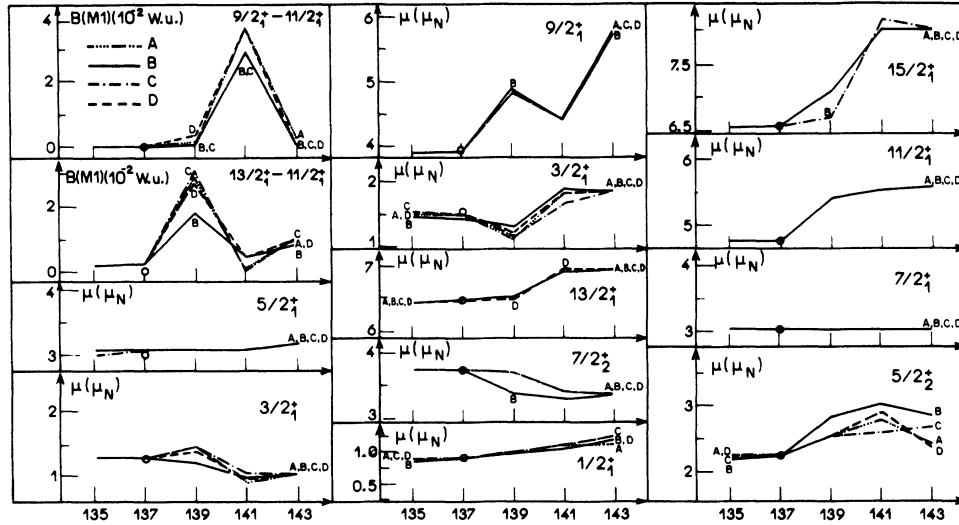


FIG. 14. Calculated magnetic dipole moments in units of n.m. for some low-lying levels of the  $N = 82$  isotones as a function of the mass number  $A$  ( $135 \leq A \leq 143$ ). Calculated  $M1$  transition rates in units of  $10^{-2}$  W.u. are also presented for two transitions. The results from the LSSM, BCS, BBCS, and PBCS approximations are labeled with the letters  $A$ ,  $B$ ,  $C$ , and  $D$ , respectively. The results calculated within the framework of the CSM are represented by open circles. The remaining  $M1$  transitions are not discussed, since they are very weak ( $10^{-3}$  W.u.) as a consequence of  $l$  forbiddenness.

The energy spectra of the  $N = 82$  nuclei, up to an excitation energy of 2 MeV, shown in Figs. 6–9, clearly demonstrate that the effects induced by low-seniority configurations with  $N_{qp} \geq 5$  are relatively small. As a matter of fact, the LSSM and the PBCS calculations generate the same number of states, the ordering of levels is practically the same and the energy differences are  $\leq 50$  keV.

To some extent the above statement is also valid for the electromagnetic properties illustrated in Figs. 14–16.

There are no significant differences for the magnetic moments and transitions and the electric observables when the states involved have  $\bar{\nu} \approx 1$ , i.e., the levels  $\frac{5}{2}^+$  and  $\frac{7}{2}^+$ . The differences are also small for the quadrupole moments of the remaining low-lying states and the  $B(E2)$  values between states with  $\bar{\nu} \approx 1$  and  $\bar{\nu} \approx 3$ . Only when both the initial and the final states are predominantly of  $\nu = 3$  character are the  $E2$  transitions evaluated within the PBCS approximation appreciably less collective than those obtained within the LSSM space.

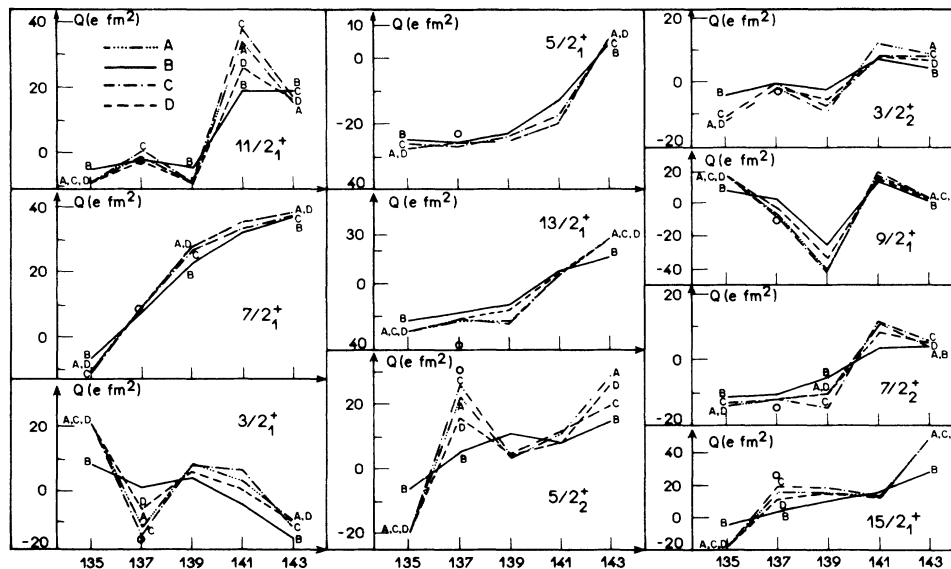


FIG. 15. Calculated electric quadrupole moments in units of  $e \text{ fm}^2$  for some low-lying levels of  $N = 82$  isotones as a function of the mass number  $A$  ( $135 \leq A \leq 143$ ). For further explanation see the caption to Fig. 14.

### C. Effects of blocking and particle-number projection

We now analyze and discuss the differences between the results obtained with the BBCS and PBCS approximations and those of the usual BCS approach. As a reference frame we use the LSSM results. In the case of three-valence particles it is easier to perform a shell-model calculation than to make use of any of the BCS approximations. Therefore we will limit our discussion to nuclei with more than three valence particles. However, for completeness, the results for  $^{59}\text{Ni}$ ,  $^{63}\text{Ni}$ , and  $^{135}\text{I}$  nuclei are also shown in figures and tables of the present work.

For the energy spectra of  $^{61}\text{Ni}$  and  $^{63}\text{Ni}$  up to an excitation energy of 2 MeV there are no significant differences between the BCS, BBCS, and PBCS results (see Figs. 2 and 3). Above 2 MeV, and when compared with the LSSM, the ordering of the states is different for each of

the three BCS approximations. The best agreement with the LSSM spectra are obtained with the PBCS method and the poorest with the BCS approach. Up to 3 MeV the largest differences in excitation energies are of the order of 250 keV.

In Table III we list the wave functions of a few low-lying states in  $^{61}\text{Ni}$  and  $^{63}\text{Ni}$  obtained with the different BCS approaches. One sees that for predominantly  $\nu=1$  states ( $\frac{1}{2}^-$ ,  $\frac{3}{2}^-$ , and  $\frac{5}{2}^-$ ) the wave functions are not very sensitive to either the effects of blocking or of particle-number projection. Conversely, the wave functions of the remaining states are rather sensitive to both effects. It should be noted that the BBCS wave functions resemble the corresponding PBCS wave functions more than the BCS wave functions. The differences in amplitudes of the wave functions are more pronounced for  $^{61}\text{Ni}$  than for  $^{63}\text{Ni}$ . For  $^{61}\text{Ni}$  they are of the order of 10%, but may be as large as 25% (compare, for example, the amplitude

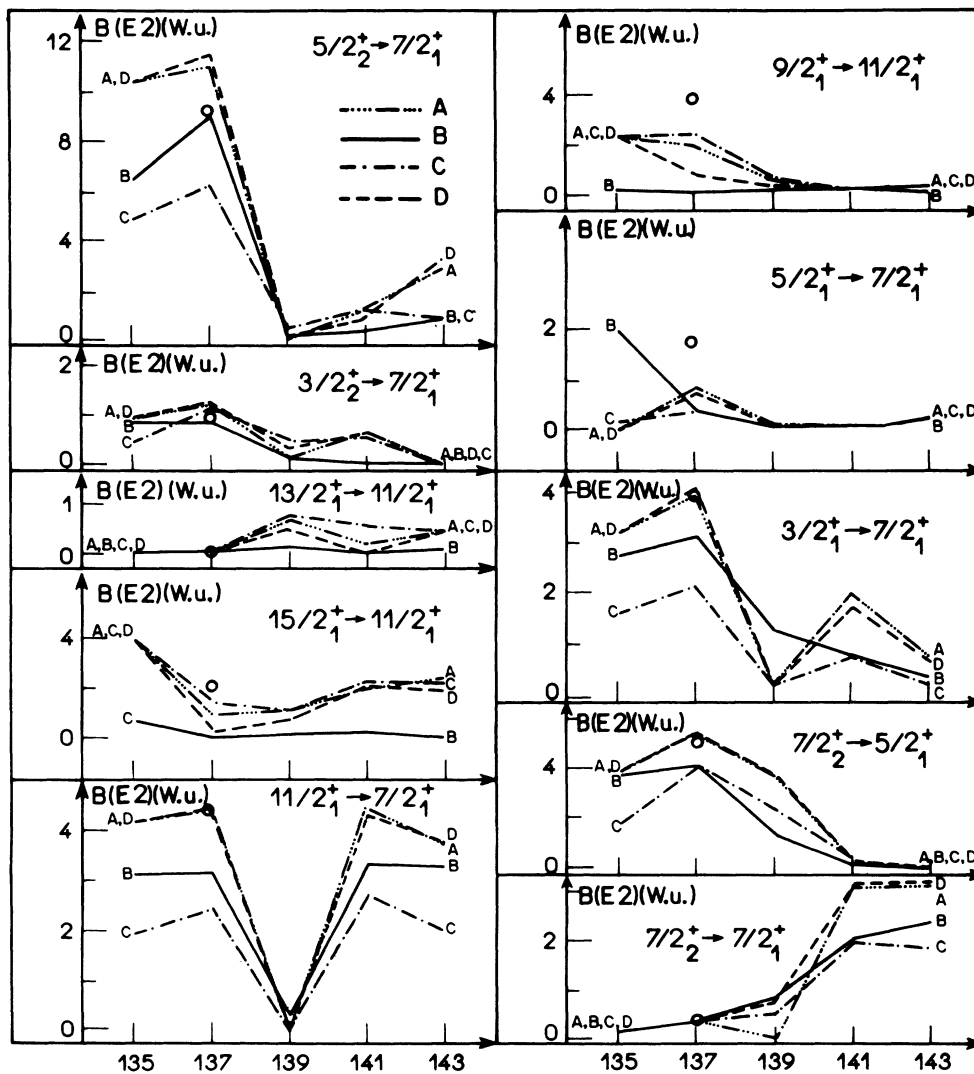


FIG. 16. Calculated  $E2$  transition rates in Weiskopf units for some transitions in  $N=82$  isotones as a function of the mass number  $A$  ( $135 \leq A \leq 143$ ). For further explanation see the caption to Fig. 14.

of the  $[(p_{3/2})^2 4, p_{1/2}]$  configuration in the  $\frac{7}{2}^-$  state). For  $^{63}\text{Ni}$  the differences are of the order of 4%.

This model dependence of the wave functions is reflected in the magnitudes of the electromagnetic observables presented in Figs. 10–13. This dependence is more notable for the electric than the magnetic observables. When compared with the LSSM results the BCS approximation exhibits significant differences in magnitude for several moments and transitions which involve the  $\frac{7}{2}^-$  level in  $^{61}\text{Ni}$  [ $\mu(\frac{7}{2}^-)$ ,  $Q(\frac{7}{2}^-)$ ,  $B(M1; \frac{7}{2}^- \rightarrow \frac{5}{2}^-)$ , and  $B(E2; \frac{7}{2}^- \rightarrow \frac{3}{2}^-)$ ] and the  $\frac{3}{2}^-$  level in  $^{63}\text{Ni}$  [ $Q(\frac{3}{2}^-)$ ,  $B(M1; \frac{3}{2}^- \rightarrow \frac{1}{2}^-)$ , and  $B(E2; \frac{3}{2}^- \rightarrow \frac{5}{2}^-)$ ]. For both nuclei the PBCS results are closer to the LSSM calculations than are those obtained with the BBCS approach.

From the energy spectra of  $N = 82$  nuclei displayed in Figs. 6–9 it can be seen that the simple BCS calculations, when compared with the results of the LSSM, yield significant differences (up to  $\approx 300$  keV) for the excitation energies of several states. As well, they yield quite different level orderings. The last effect is particularly accentuated in the energy regions where the level densities are rather high. Although both the BBCS and the PBCS approaches provide satisfactory results for the energy spectra, the PBCS results are in somewhat better agreement with the LSSM calculations.

In Table VI the wave functions of  $N = 82$  isotones with more than five valence particles calculated with the different BCS approximations are compared with each other. For predominantly 1qp states, i.e., the  $\frac{5}{2}^+$  and  $\frac{7}{2}^+$  levels, all three calculations yield similar wave-function amplitudes. For the remaining states only the BBCS and PBCS amplitudes are close to each other. The most noticeable differences between the BCS and the BBCS (or PBCS) wave functions occur for the  $[(\frac{7}{2})^2 J, \frac{5}{2}]$  configurations in  $^{139}\text{La}$  and for the  $[(\frac{5}{2})^2 J, \frac{7}{2}]$  configurations in  $^{141}\text{Pr}$ .

The results for the electromagnetic properties calculated with these wave functions are compared with the LSSM results in Figs. 14–16. It is seen that all four models furnish similar results for the magnetic observables. The most notable discrepancy is found in the BCS value for the  $\frac{13}{2}^+ \rightarrow \frac{11}{2}^+$   $M1$  transition in  $^{139}\text{La}$ . Among all the BCS results for the electric observables, only those for  $Q(\frac{5}{2}^+)$ ,  $Q(\frac{7}{2}^+)$ , and  $B(E2; \frac{5}{2}^+ \rightarrow \frac{7}{2}^+)$  are close to the LSSM results. On the other hand, the electric quadrupole results obtained within the PBCS and BBCS approaches are not substantially different from those obtained with the LSSM. With respect to the  $B(E2)$  values it should be noted that the best overall agreement is achieved with the number-projection method. It is also important to note that when a  $B(E2)$  value strongly fluctuates in going from one nucleus to another, as happens in the case of the  $\frac{5}{2}^+ \rightarrow \frac{7}{2}^+$ ,  $\frac{3}{2}^+ \rightarrow \frac{7}{2}^+$ , and  $\frac{11}{2}^+ \rightarrow \frac{7}{2}^+$  transitions, the ordinary BCS calculations lead to more satisfactory results than do the BBCS calculations.

We have mentioned that in most instances the electric observables are more sensitive to the effects of blocking and number projection than are the magnetic observables. We clarify this point with a qualitative discussion of the matrix elements of the one body operator  $T_\lambda$ . We

assume that both the initial and final wave functions are predominantly of 1qp or 3qp character (see Tables III and VI). Therefore the following matrix elements will appear:

$$(i) \langle \psi(1qp) || T_\lambda || \psi'(1qp) \rangle,$$

$$(ii) \langle \psi(1qp) || T_\lambda || \psi(3qp) \rangle, \text{ and}$$

$$(iii) \langle \psi(3qp) || T_\lambda || \psi(3qp) \rangle.$$

The matrix element of the type (i) and (iii) are proportional to the scattering pairing factor  $F_s(\lambda) \equiv [u_a u_b' - (-)^{\lambda} v_a v_b']$  and those of the type (ii) to the pair creation pairing factor  $F_p(\lambda) \equiv [u_a' v_b' - (-)^{\lambda} v_a' u_b']$ . One may distinguish two limiting situations: (1) the valence shell is approximately half-filled in which case the electric pairing factors are  $F_s(\lambda=2) \approx 0$  and  $F_p(\lambda=2) \approx 1$ ; (2) only a few particles or holes are in the valence shell and therefore  $F_s(\lambda=2) \approx 1$  and  $F_p(\lambda=2) \approx 0$ . In both limiting situations the magnetic pairing factors are  $F_s(\lambda=1) \approx 1$  and  $F_p(\lambda=1) \approx 0$ . On the other hand, the results for the electromagnetic prop-

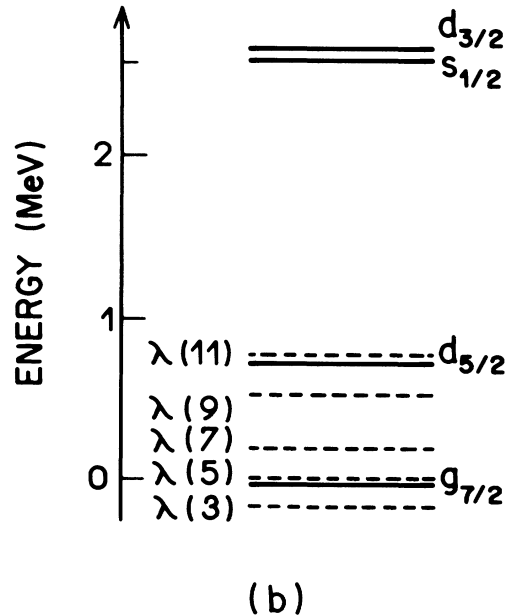
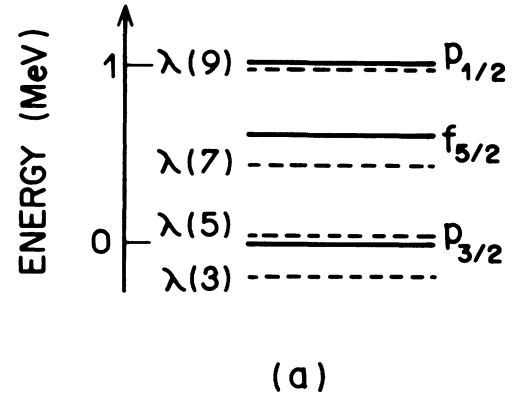


FIG. 17. Single-particle energies (solid line) and Fermi energies (dashed line)  $\lambda(n_0)$  where  $n_0$  is the number of nucleons for Ni isotopes (a) and for  $N = 82$  isotones (b).

erties shown in Figs. 10–13 and 14–16, correspond mostly to the case (1) and thus the blocking effect is particularly relevant for the electric observables of types (i) and (iii) and for the magnetic observables of type (iii).

It is clear that the main differences between the BCS and BBCS results arise from differences in the gap parameter. This quantity diminishes with the effects of blocking and becomes configuration dependent. Moreover, as shown in Ref. 17, the pairing reduction depends sensitively on the single-particle level distribution near the Fermi surface and is particularly pronounced when the blocked level is located close to the Fermi surface. Thus, from the results shown in Fig. 17, one can easily convince oneself that the blocking effect is very important for the following wave-function amplitudes (and the corresponding electromagnetic observables): (i) configurations which contain two particles in the  $p_{3/2}$  single particle state and participate in building up the wave functions of  $^{61}\text{Ni}$  and (ii) components which involve the  $g_{7/2}$  orbital in  $^{137}\text{Cs}$  and  $^{139}\text{La}$  and the  $d_{5/2}$  orbital in  $^{141}\text{Pr}$  and  $^{143}\text{Pm}$ ; the effect is particularly relevant for the configurations  $|(\frac{7}{2})^2J, \frac{5}{2}\rangle$  in  $^{139}\text{La}$  and the configurations  $|(\frac{5}{2})^2J, \frac{7}{2}\rangle$  in  $^{141}\text{Pr}$ .

However, conversely to what one would expect, the structures of  $^{137}\text{Cs}$  and  $^{143}\text{Pm}$  seem to be less affected by the blocking than those of  $^{139}\text{La}$  and  $^{141}\text{Pr}$  (see Fig. 17). This fact indicates that a discussion of the blocking effect based only on the analysis of a few diagonal matrix elements of  $H$  and/or on the most important contributions to  $T_\lambda$  might be a oversimplification and inconclusive.

## V. CONCLUSIONS

A detailed study of the effects upon the BCS approximation which are introduced by corrections for particle-number projection and blocking has been carried out by using the low-seniority shell-model as the frame of reference with which to investigate the mixing of one and three-quasiparticle states in Ni isotopes and in  $N=82$  isotones. In addition, the effects of seniority-five

configurations on low-lying states has also been studied through the comparison of low-seniority shell-model results with those which arise from the full shell-model calculations. The following general conclusions can be drawn from this study.

(1) A BCS approximation which includes corrections either for particle-number projection or blocking yields results which are in most respects very similar to results obtained with the low-seniority shell model.

(2) The five-quasiparticle configurations with seniority one and three do not play an important role in the structure of low-lying states.

(3) The effects of seniority-five configurations upon the electromagnetic processes can be significant even among the lowest-lying states and cannot be accounted for through an overall renormalization of the residual interaction or by the use of effective charges.

We have several calculations which include particle-number projection and the blocking simultaneously. These calculations are significantly more time consuming than are the BBCS and PBCS methods separately, but they do not yield appreciably better results than do the individual BBCS and PBCS approaches. Thus, it does not appear to be profitable to make both of these corrections to the BCS method.

We have not presented a comparison between the experimental data and any of these calculations, but with the parametrization listed in Sec. III, the complete shell-model (CSM) yields a reasonable good overall agreement with experimental data.

## ACKNOWLEDGMENT

This work was supported in part by the U.S. National Science Foundation under Grant No. PHY-87-18772, by Fundação de Amparo a Pesquisa do Estado de São Paulo, by Conselho Nacional de Desenvolvimento Científico e Tecnológico, and By Consejo Nacional de Investigacion Científica y Tecnológica.

<sup>1</sup>T. T. S. Kuo, E. U. Baranger, and M. Baranger, *Nucl. Phys.* **79**, 513 (1966).  
<sup>2</sup>K. Dietrich, H. J. Mang, and J. H. Pradal, *Phys. Rev.* **135**, 322 (1964).  
<sup>3</sup>P. L. Ottaviani and M. Savoia, *Phys. Rev.* **187**, 1306 (1969); *Nuovo Cimento* **67A**, 630 (1970); *Phys. Rev.* **178**, 1594 (1969).  
<sup>4</sup>K. Allaart and E. Boeker, *Nucl. Phys.* **A168**, 630 (1971); **A198**, 33 (1972).  
<sup>5</sup>K. Allaart and W. F. Van Gunsteren, *Nucl. Phys.* **A234**, 53 (1974).  
<sup>6</sup>I. N. L. Akkermans, K. Allaart, and Z. Boeker, *Nucl. Phys.* **A282**, 291 (1977).  
<sup>7</sup>S. G. Nilsson, *Nucl. Phys.* **55**, 97 (1964).  
<sup>8</sup>H. Dias and F. Krmpotić, *Phys. Lett.* **112B**, 103 (1982).  
<sup>9</sup>L. Losano, H. Dias, F. Krmpotić, and B. H. Wildenthal (unpublished).

<sup>10</sup>J. B. French, E. C. Halbert, J. B. Mcgrory, and S. S. M. Wong, *Adv. Nucl. Phys.* **3**, 193 (1969).  
<sup>11</sup>M. H. Macfarlane, *Lectures in Theoretical Physics* (University of Colorado Press, Boulder, 1966), p. 583.  
<sup>12</sup>H. Dias, Ph.D. thesis, University of São Paulo, 1980 (unpublished).  
<sup>13</sup>A. Plastino, R. Arvieu, and S. A. Moskowski, *Phys. Rev.* **145**, 837 (1966).  
<sup>14</sup>N. Freed and N. Miles, *Nucl. Phys.* **A167**, 230 (1970).  
<sup>15</sup>L. S. Kisslinger and R. A. Sorensen, *Rev. Mod. Phys.* **35**, 853 (1963).  
<sup>16</sup>J. E. Koops and P. W. M. Glaudemans, *Z. Phys. A* **280**, 181 (1977).  
<sup>17</sup>J. Y. Zeng, T. S. Cheng, L. Cheng, and C. S. Wu, *Nucl. Phys.* **A411**, 49 (1983).